patterned site fidelity after six layers. The pattern spacing affects the QD dimensions, and measuring QD size with increasing pattern spacing provided an estimation of the maximum adatom diffusion length, which is determined by the particular growth conditions. Patterning also provided the ability to alter the WL thickness. Additionally, the size of the FIB-milled holes affects QD diameter and pattern fidelity. Mound formation upon increasing the total number of layers to 26 was detrimental to pattern fidelity, and created a bimodal QD size distribution for most larger pattern spacings as measured by AFM and evidenced by a split QD PL peak.

3.5 References

[1] A. Luque, and A. Marti *Physical Review Lett.* **78** 26 5014 (1997).

[2] A. Marti, N. Lopez, E. Antolin, E. Canovas, C. Stanley, C. Farmer, L. Cuadra, and A. Luque *Thin Solid Films* **511-512** 638-644 (2006).

[3] N. N. Ledentsov, V. A. Shchukin, M. Grundmann, N. Kirstaedter, J. Bohrer, O. Schmidt, D. Bimberg, V. M. Ustinov, A. Y. Egorov, A. E. Zhukov, P. S. Kop'ev, S. V. Zaitsev, N. Y. Gordeev, Z. I. Alferov, A. I. Borovkov, A. O. Kosogov, S. S. Ruvimov, P. Werner, U. Gosele, and J. Heydenreich *Phys. Rev. B* **54** 12 8743-8750 (1996).

[4] L. Bousaiene, B. Ilahi, L. Sfaxi, F. Hassen, H. Maaref, O. Marty, and J. Dazord *Appl. Phys. A* **79** 587-591 (2004).

[5] D. Englund, D. Fattal, E. Waks, G. Solomon, B. Zhang, T. Nakaoka, Y. Arakawa, Y. Yamamoto, and J. Vuckovic *Phys. Rev. Lett*. **95** 013904 (2005).

[6] A. Badolato, K. Hennessy, M. Atature, J. Dreiser, E. Hu, P. M. Petroff, and A. Imamoglu *Science* **308** 1158 (2005).

[7] H. McKay, P. Rudzinski, A. Dehne, and J. M. Millunchick *Nanotechnology* **18** No. 455303 (2007).

[8] P. Atkinson, O. G. Schmidt, S. P. Bremner, and D. A. Ritchie *C.R. Physique* **9** 788-803 (2008).

[9] Y. Nakamura, O. G. Schmidt, N. Y. Jin-Phillip, S. Kiravittaya, C. Muller, K. Eberl, H. Grabeldinger, and H. Schweizer *Journal of Crys. Growth* **242** 339-344 (2002).

[10] A. Portavoce, R. Hull, M. C. Reuter, and F. M. Ross *Physical Rev. B* **76** 235301 (2007).

[11] R. Hull, J. F. Graham, A. J. Kubis, A. Portavoce, and F. M. Ross *Microscopy and Microanalysis* **13** (Suppl 2) (2007).

[12] M. Gherasimova, R. Hull, M. C. Reuter, and F. M. Ross *Appl. Phys. Lett.* **93** 023106 (2008).

[13] J. Y. Lee, M. J. Noordhoek, P. Smereka, H. McKay, and J. M. Millunchick *Nanotechnology* **20**, No. 285305 (2009).

[14] J. Lee, T. W. Saucer, A. J. Martin, D. Tien, J. M. Millunchick, and V. Sih *Nano Lett.* **11** 1040-1043 (2011).

[15] M. Mehta, D. Reuter, A. Melnikov, A. D. Wieck, and A. Remhof *App. Phys. Lett.* **91** 123108 (2007).

[16] M. Mehta, D. Reuter, A. Melnikov, A. D. Wieck, and A. Remhof *Physica E* **40** 2034-2036 (2008).

[17] S. Kiravittaya, M. Benyoucef, R. Zapf-Gottwick, A. Rastelli, and O. G. Schmidt *Appl. Phys. Lett*. **89** 233102–233104 (2006).

[18] S. Kiravittaya, H. Heidemeyer, and O. G. Schmidt *Physica E* **23** 253-259 (2004).

[19] T. W. Saucer, J. Lee, A. J. Martin, D. Tien, J. M. Millunchick, and V. Sih *Solid State Commun*. **151** 269–271 (2011).

[20] C. C. Cheng, K. Meneou, and K. Y. Cheng *J. of Cryst. Growth* **323** 180-182 (2011).

[21] S. Kiravittaya, A. Rastelli, and O. G. Schmidt *Rev. Prog. Phys.* **72** 046502 (2009).

[22] Q. Xie, A. Madhukar, P. Chen, and N. P. Kobayashi *Phys. Rev. Lett.* **75** 2542-2545 (1995).

[23] P. Howe, E. C. Le Ru, E. Clarke, B. Abbey, R. Murray, and T. S. Jones *J. of Appl. Phys.* **95** 6 (2004).

[24] M. Gutierrez, M. Herrera, D. Gonzalez, and R. Garcia *Appl. Phys. Lett.* **88** 193118 (2006).

[25] I. Levchenko, and K. Ostrikov *Appl. Phys. Lett.* **95** 243102 (2009).

[26] A. Pimpinelli, and T. L. Einstein *Phys. Rev. Lett.* **99** 226102 (2007).

[27] Z. R. Wasilewski, S. Fafard, and J. P. McCaffrey *J. of Crys. Gr.* **201/202** 1131-1135 (1999).

Chapter 4

Effects of Pre-Determined Lateral Separation on Quantum Dot Size and Dissolution

Placing quantum dots in precise arrays provides a unique environment in which to study the effects of surface energy driven quantum dot dissolution occurring during capping, which is difficult to study using randomly assembled dots. Quantum dot photoluminescence emission energy is shown to initially decrease with increasing pattern spacing, but then increases for separations greater than 1.0 μm. The shift in photoluminescence emission results from a competition between the effects of dot size and those of dissolution on the dot emission energy. This data also demonstrates the difference in the diffusion length of In on InAs and on GaAs.

4.1 Introduction

Semiconductor quantum dots (QD) are of interest for applications such as solar cells,[1,2] lasers,[3,4] and quantum information processing.[5] III-V QDs are typically grown by self-assembly via the Stranski-Krastanov growth mode where QD position is random and the areal density and size are controlled by the growth parameters (e.g., deposition rate, growth temperature, amount of material deposited for the QD). For certain applications it can be advantageous to precisely control the QD dimensions and areal density because these properties directly influence their optical and electronic properties. For example, controlling the QD dimensions provides a means of tailoring the transition energy of the dots, which is critical in telecommunications

applications.[4,6] Additionally, precise positioning of QDs is beneficial for some quantum computing devices where QDs can be coupled to a photonic crystal cavity.[5,7,8]

Lateral patterning of the growth surface using a focused ion beam (FIB) has been used to achieve QD nucleation below the critical thickness at patterned locations due to changes in strain and surface topography at these sites.[9-11] Because the QDs nucleate only at the FIB-milled sites, altering the pattern spacing provides a means of controlling QD areal density. Additionally, FIB patterning of InAs/GaAs QDs has been demonstrated as an effective way of controlling QD dimensions. QD diameter and height have been shown to increase with increasing pattern spacing until the pattern spacing surpasses the In adatom surface diffusion length for the given growth conditions, at which point the dimensions plateau.[10] The ability of FIB patterning to create arrays of QDs with a predetermined separation distance provides a unique environment in which to study the properties of individual QDs as well as the effects of separation distance on their optical properties.[10-13] As a result, macro- and micro-photoluminescence have been previously measured for FIB-patterned InAs/GaAs QDs.[9-14] Additionally, single QD emission with a line width of 160 μeV has been measured from FIB-patterned QDs with a large separation distance.[11,12] This chapter presents analysis of the effects of separation distance on the size and dissolution of laterally patterned InAs/GaAs QDs.

4.2 Experimental Procedure

A multilayer InAs QD structure consisting of six layers was grown by molecular beam epitaxy (MBE) on a GaAs(001) substrate that was laterally patterned using an *in vacuo* FIB. First, a 500 nm GaAs buffer layer was grown at $T = 590\ ^{o}C$. After buffer growth, the sample was transferred *in vacuo* to the FIB for patterning of 40 x 40 μm^2 arrays of holes, which were FIB-milled with a single pass of a 10 pA, 30 keV Ga^+ ion beam. A total of 12 unique patterns were

made using FIB dwell times of 3.0, 6.0, and 9.0 ms, each at pattern spacings of 0.25, 0.5, 1.0, and 2.0 μm. The specific dwell time used determines the depth and width of the FIB-milled holes. The sample was transferred *in vacuo* back to the MBE after patterning. 2.0 monolayers (ML) of InAs was deposited for the QDs at $T = 485\ ^{o}C$ and a rate of 0.11 MLs^{-1}. The QDs were immediately capped with 20 nm of GaAs at a rate of 1.0 MLs^{-1}. The InAs QD growth and GaAs capping processes were repeated to form a six-layer QD structure. However, lateral patterning was done only at the substrate, prior to the first layer of QDs. The topmost layer of QDs remained uncapped for analysis by atomic force microscopy (AFM). For photoluminescence (PL) analysis, the sample was mounted in a helium flow cryostat at 15 K and pumped using a 633 nm helium-neon laser with 101 μW incident power focused through a 0.7 NA infinity corrected objective. The PL spectra were collected using a 0.75 m spectrometer with a 150 G/mm reflection grating and a CCD detector.

4.3 Data Analysis

4.3.1 Effects of FIB Pattern Spacing on QD Dimensions and Fidelity

In the previous chapter, we examined the effects of lateral FIB patterning on uncapped QD dimensions, wetting layer thickness, and pattern fidelity for multilayer QD structures.[10] In this paper, we examine in detail the effects of lateral FIB patterning on dot size and dissolution via PL. A summary of the key findings of the previous chapter that are relevant to this chapter is first described. The effects of patterning are retained at the sixth layer despite being FIB-milled only at the substrate. Figure 4.1 shows an AFM image of the uncapped, top layer of the pattern with a 9 ms FIB dwell time and 2.0 μm spacing. The size of the FIB-patterned holes and the spacing between them directly influences the QD dimensions. The QD dimensions and wetting

layer thickness increase with increasing pattern spacing. Figure 4.2 shows plots of the average uncapped QD diameter and height with respect to increasing pattern spacing for the patterns with a 9 ms FIB dwell time. Note that the data points for QD height in Figure 2 are slightly offset in *x* in order to more clearly display the data. For the 9 ms FIB dwell time, the average uncapped QD diameter increases from 45 ± 14 nm to 91 ± 28 nm, and the average height increases from 6 ± 3 nm to 15 ± 6 nm for pattern spacings of 0.25 to 2.0 μm, respectively. The QD diameter and height saturate after the pattern spacing exceeds approximately 1.0 μm. This results because the pattern spacing exceeds the In adatom surface diffusion length during dot nucleation, therefore, limiting the maximum QD size obtainable under the given growth conditions (i.e., growth temperature, growth rate, deposited InAs thickness).[10]

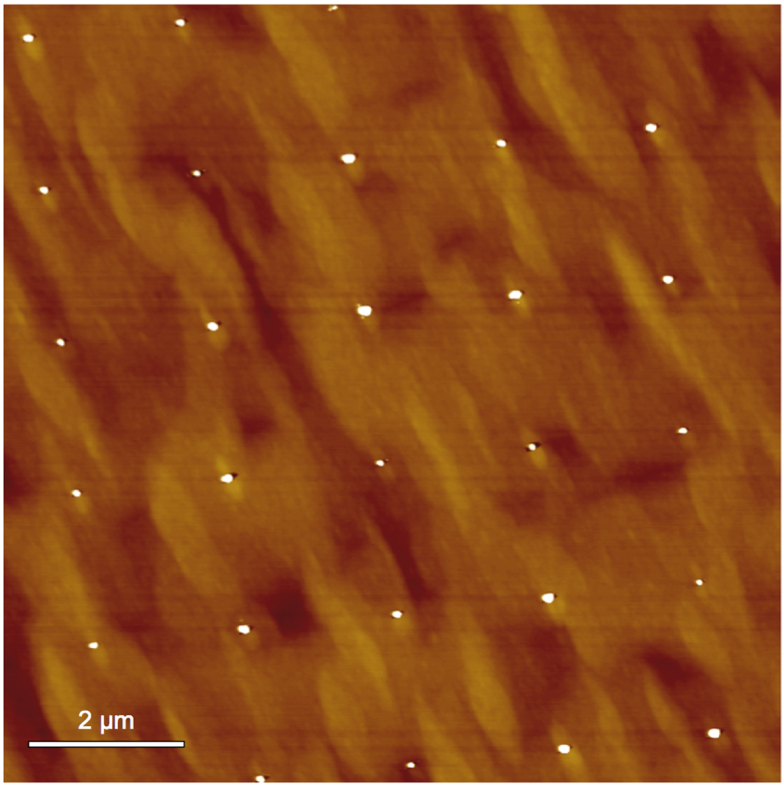

Figure 4.1: Atomic force microscope image of the top layer of a six-layer stack of quantum dots patterned with a 10 pA, 30 keV Ga^+ *in vacuo* focused ion beam with a 9.0 ms dwell time and a 2.0 μm pattern spacing.

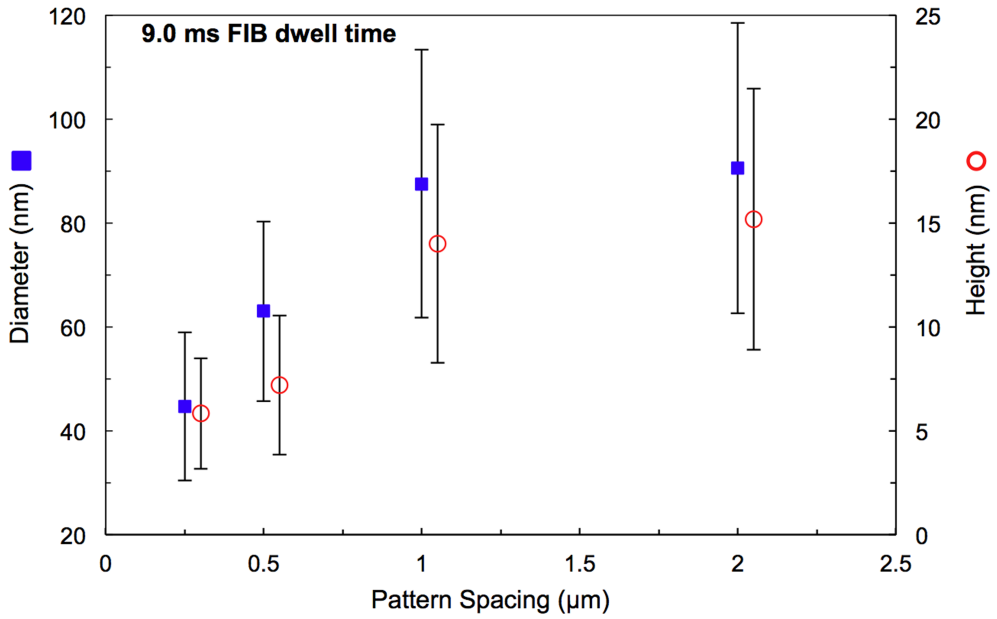

Figure 4.2: Plot of quantum dot diameter and height for the 9.0 ms dwell time patterns as a function of pattern spacing. Note that the height data points are offset slightly in *x* to more clearly display the data.

4.3.2 Changes in Photoluminescence Energy as a Function of Pattern Spacing

Figure 4.3 shows the PL spectrum from the 9 ms FIB dwell time pattern for each of the four pattern spacings and for the unpatterned region. The GaAs substrate peak is at approximately 1.48 eV, the wetting layer peak ranges from 1.43 to 1.45 eV, and the QD peak ranges from 1.34 to 1.39 eV for the different pattern spacings. For each FIB dwell time, the wetting layer PL peak shifts to lower energy with increasing pattern spacing and, for the 1.0 and 2.0 μm pattern spacings, approaches that of the unpatterned region. Figure 4.4 (a) shows a plot of the wetting layer PL peak energy for each FIB dwell time as a function of the pattern spacing. This is consistent with the prior finding that the wetting layer thickness increases with increasing pattern spacing,[10] therefore, causing a shift in emission energy. Additionally, the relative intensity of the wetting layer PL peak also increases with pattern spacing and approaches that of

the unpatterned region. This is expected due to the increase in area of the wetting layer and the decrease in QD areal density as the pattern spacing increases.[13] Figure 4.5 shows plots of the wetting layer and QD PL intensities relative to the GaAs peak as a function of pattern spacing.

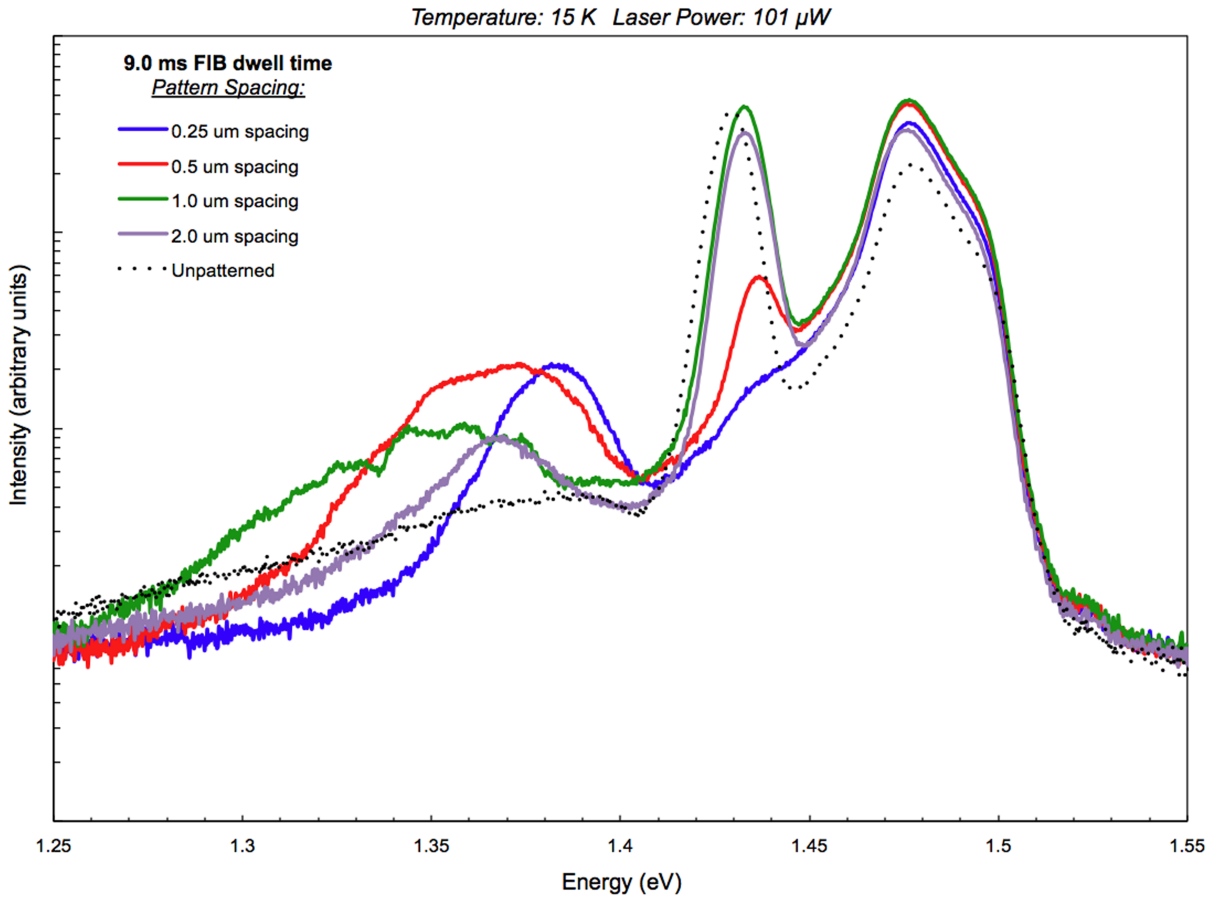

Figure 4.3: Photoluminescence data for the 9.0 ms dwell time patterns at each pattern spacing and for the unpatterned regions. Measurements were taken at 15 K and 101 μW laser power. The GaAs substrate peak is at 1.48 eV, the wetting layer peak ranges from 1.43 to 1.45 eV, and the QD peak ranges from 1.34 to 1.39 eV dependent on the pattern spacing. Data collected by Timothy W. Saucer, Prof. Vanessa Sih group, Physics Department, University of Michigan.

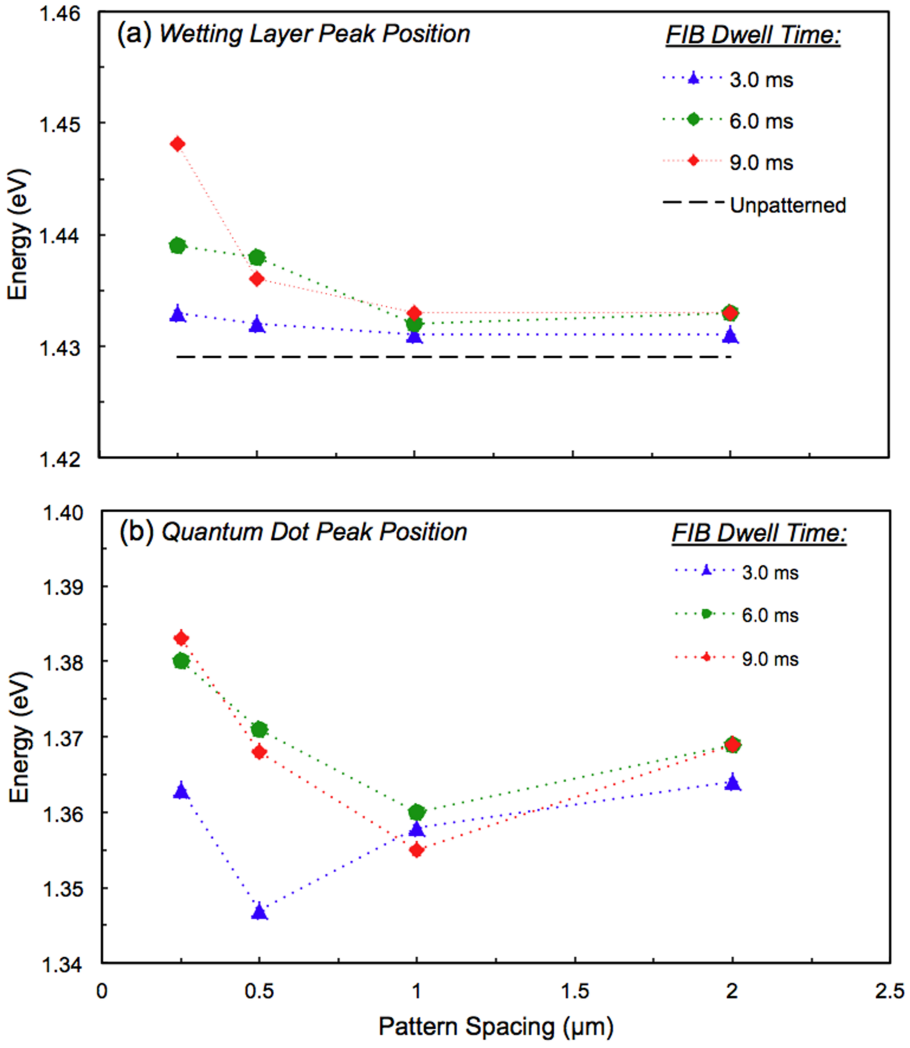

Figure 4.4: Plots of (a) wetting layer and (b) quantum dot photoluminescence peak energy as a function of pattern spacing for each dwell time. The dashed line in (a) shows the peak energy for the unpatterned region.

The PL emission from the QDs behaves somewhat differently than that of the wetting layer. Initially, the QD PL peak position (Figure 4.3) also shifts to lower energy with increasing pattern spacing. However, at the 2.0 μm pattern spacing the peak position shifts back to higher energy. Figure 4.4 (b) shows a plot of the QD PL peak energy as a function of pattern spacing for each FIB dwell time. For each FIB dwell time, the QD PL peak position follows this same "U"-shaped trend, decreasing in energy initially and then increasing at larger pattern spacings. Based

on the QD dimensions alone, the PL peak energy is not expected to change for pattern spacings beyond 1.0 μm because the dimensions of uncapped QDs remain constant beyond this point. Therefore, it is expected to follow a similar trend to that of the wetting layer.

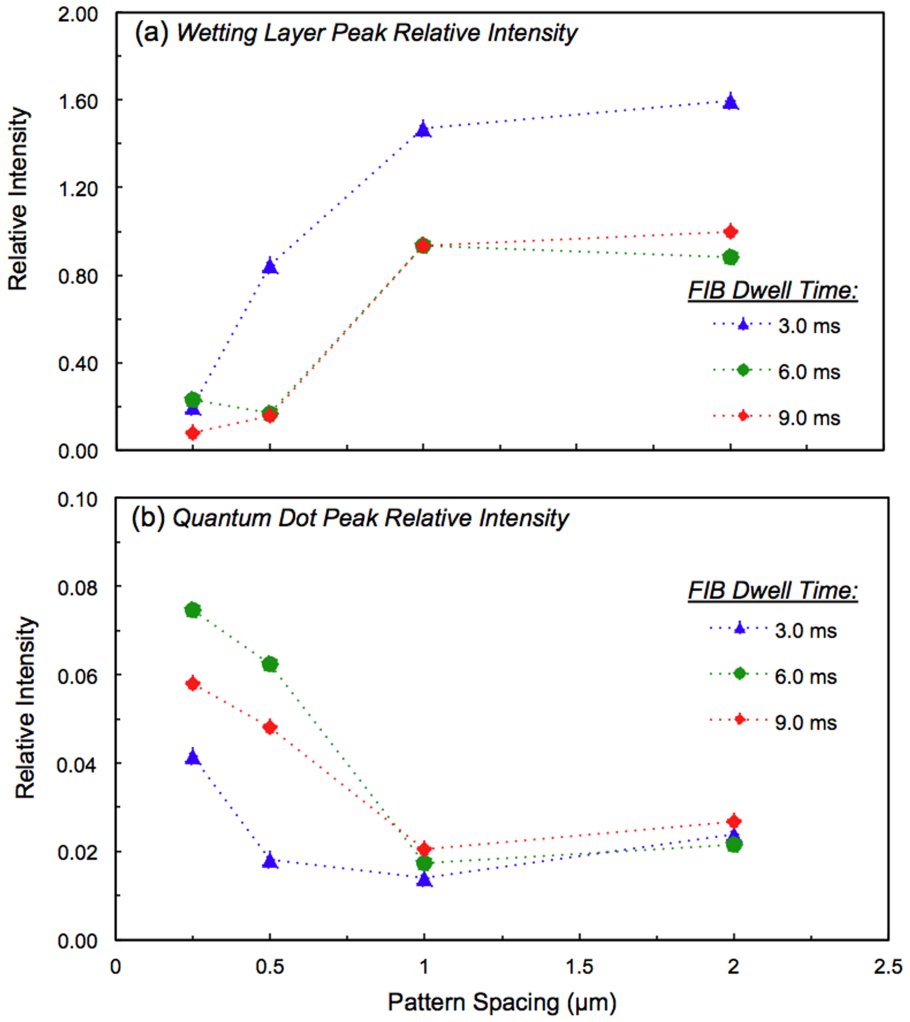

Figure 4.5: Plots of (a) wetting layer and (b) quantum dot photoluminescence peak intensity relative to the GaAs peak intensity as a function of pattern spacing for each dwell time.

4.3.3 QD Dissociation Due to Increasing Separation

This data suggests that there is a competing mechanism that alters the QD PL emission as dot separation increases. There are several factors that can cause QD PL emission to shift to

higher energy. Three primary factors are: QD dimensions, strain, and QD composition. As the size of the QDs increases, their PL emission energy is expected to decrease due to reduced quantum confinement. This effect is evident for the 0.25 to 1.0 μm pattern spacings where there is a strong correlation between the QD dimensions and their PL emission energy. However, the uncapped QD dimensions for the 2.0 μm pattern spacing do not differ from those of the 1.0 μm spacing, so no change (neither increase nor decrease) in QD PL emission energy as a result of QD size is expected for pattern spacings larger than 1.0 μm. Strain can also affect the QD PL emission energy, however, the effects of strain on the band gap of the dots should be the same for a given FIB dwell time and independent of the pattern spacing.

It is well known that capping of QDs can alter their size, shape, and composition, which can affect their optoelectronic properties. Dissolution of InAs QDs during capping has been demonstrated experimentally using cross-sectional scanning tunneling microscopy[15,16] and simulated using Kinetic Monte Carlo (KMC).[17,18] It has been found that the driving force for QD dissolution during capping stems from the difference in surface energy between the QD material and that of the cap.[18] To better understand this, it is helpful to consider the factors influencing wetting layer formation and QD nucleation. Upon initial InAs deposition, the primary driving force is to wet the GaAs surface to reduce the surface energy. Once the GaAs surface is covered, continued film growth creates increasing strain due to the lattice mismatch between InAs and GaAs. This strain creates a driving force for dot nucleation once a critical thickness is exceeded. During GaAs capping of the dots, the InAs wetting layer becomes covered with higher surface energy GaAs. Because the driving force to reduce surface energy is strong, In diffuses from the QDs to cover the GaAs surface, resulting in dissolution of the QDs and a reduction of average size and/or In composition within the dots.[18-20] The driving force for QD dissolution is limited by

the amount of available GaAs surface area. Based upon this, a higher degree of dissolution is expected as QD separation increases due to the increased GaAs surface area between QDs during capping.

The patterned QDs presented in this study provide a unique environment in which to study this phenomenon. In the case of randomly assembled QDs, the effects of surface energy driven QD dissolution are difficult to observe because the separation between QDs cannot be predetermined nor held constant. The creation of large, patterned arrays of QDs with a predetermined spacing allows for systematic studies of their structure-property relationships. The shift in PL emission energy with increasing pattern spacing is a result of the competition between the effects of QD size dictated by the pattern spacing and those of dot dissolution upon capping. At smaller pattern spacings, the effects of QD size on the PL emission energy dominate over those of dissolution, but at larger pattern spacings, the effects of QD dissolution dominate. It is unclear whether the QD dissolution simply results in a decrease in QD dimensions or a compositional change within the QD due to GaAs intermixing, since either will result in an increase in the PL emission energy.

4.3.4 Distinguishing Surface Diffusion Lengths via FIB Patterning

Both the QD nucleation and dissolution processes are limited by the In diffusion length, but it is important to note that this length may be different for these two processes. The size of the uncapped QDs increases as a function of pattern spacing and saturates at a pattern spacing of approximately 1.0 μm (Figure 4.2). This suggests that the diffusion length of In atoms on the InAs wetting layer surface is on the order of 500 nm for the given growth conditions, which corresponds to half the pattern spacing. The PL data shows that there is an increase in the QD PL

peak energy between the 1.0 and 2.0 μm pattern spacings, suggesting a longer In diffusion length during QD dissolution. If the diffusion length of In was the same in both cases, then the QD PL emission energy would saturate at a pattern spacing of 1.0 μm. The fact that it does not suggests that the diffusion length of In on GaAs is 1.0 μm or greater.

4.4 Conclusions

In conclusion, FIB patterning has been demonstrated as a unique method for observing changes in QD dimensions and dissolution by altering dot spacing in a controlled manner. Changes in QD dimensions and dissolution are evident via AFM and photoluminescence measurements as a function of dot spacing. An increase in both the QD dimensions and dissolution as pattern spacing increases creates a competition between a red shift and blue shift in the PL emission energy, respectively. The effects of QD size dominate at closer pattern spacings. However, dot dimensions are limited by the In diffusion length on InAs during dot nucleation and plateau at a pattern spacing of about 1.0 μm. The effects of dot dissolution dominate at the largest pattern spacing, showing that the diffusion length of In on GaAs must be larger than that of In on InAs, resulting in the blue shift in PL emission for the 2.0 μm pattern spacing.

4.5 Applications of FIB-Patterned InAs Quantum Dots

The work presented on FIB patterning of InAs/GaAs QDs is of broader interest for QD lasers,[3,4] solar cells,[1,2,21] and quantum computing. This research is a collaborative effort with Prof. Vanessa Sih's group in the Physics department at the University of Michigan. The specific goal is to understand the effects of patterning in order to laterally position InAs QDs with the optical cavity of a photonic crystal for information processing. FIB patterning is advantageous

for this work because it provides a means of tailoring QD areal density, position, and size. This makes it possible to fabricate a photonic crystal with the desired number of QDs positioned directly within the optical cavity, which emit photons with the desired wavelength.

A photonic crystal is a structure with a periodic modulation in refractive index designed to guide photons of a restricted wavelength through the structure.[22] Photonic crystals affect the propagation of photons through the photonic crystal in the same way that the periodic potential in a semiconductor affects the movement of electrons through the lattice.[22] Photonic crystals can be one-, two-, or three-dimensional. Figure 4.6 shows schematics of one-, two-, and three-dimensional photonic crystal structures taken from.[22] In this collaborative work, the focus is on two-dimensional photonic crystals.

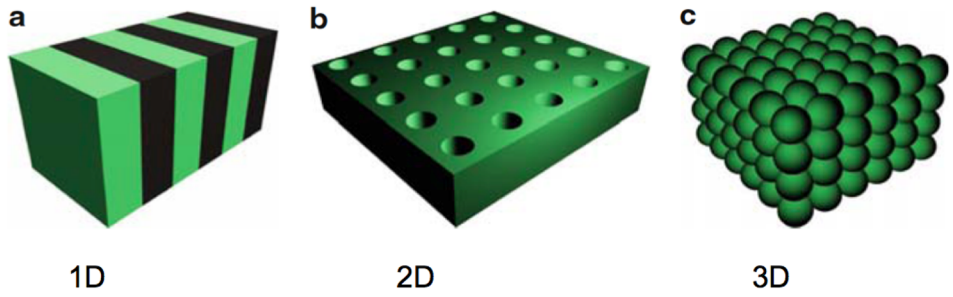

Figure 4.6: Schematics of the different types of photonic crystals. Image taken from Igor *et al*.[22]

Prior to the design and fabrication of two-dimensional photonic crystals, several studies were done on unpatterned and FIB-patterned InAs QDs in addition to the ones presented above in order to determine the patterning and growth conditions necessary to achieve the desired QD properties. These studies included altering the growth temperature, the amount of InAs deposited, and including a pre-capping annealing step for unpatterned InAs QDs. Additionally, studies were done on the effects of FIB patterning at the first, second, and third layers of QDs.[23] The effects of patterning on the initial QD layers are of interest because the QD structures

designed for the photonic crystals consist of only three layers of QDs. Initial photonic crystals were fabricated on samples containing three layers of unpatterned QDs emitting at the desired wavelength of approximately 890 nm. Figure 4.7 shows a plot of PL emission from the photonic crystal at 0^o and 90^o.[5] The inset shows a scanning electron microscope image of the two-dimensional photonic crystal. The effects of the photonic crystal are evident by lack of QD PL emission perpendicular to the long direction of the cavity.

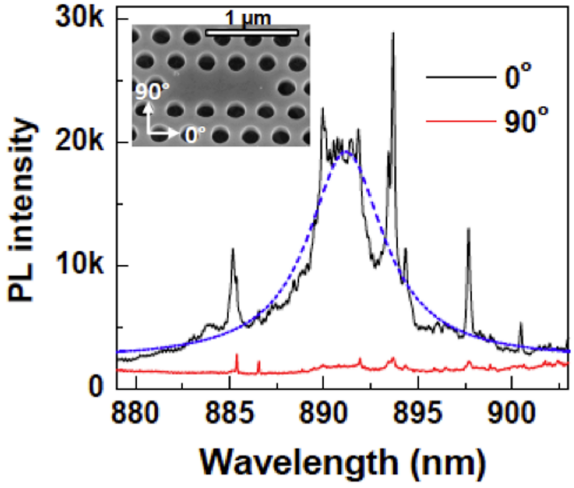

Figure 4.7: Enhancement of photoluminescence from quantum dots embedded in a photonic crystal. Spectra were measured at a laser power of 190 μW. The blue dashed line is a Lorentzian fit. The inset is a scanning electron microscope image of the photonic crystal. Figure adapted from Lee *et al.*[5]

4.6 References:

[1] A. Luque and A. Marti, Phys. Rev. Lett. 78, 26 5014 (1997).

[2] A. Marti, N. Lopez, E. Antolin, E. Canovas, C. Stanley, C. Farmer, L. Cuadra, and A. Luque, Thin Solid Films 511-512, 638 (2006).

[3] N. N. Ledentsov, V. A. Shchukin, M. Grundmann, N. Kirstaedter, J. Bohrer, O. Schmidt, D. Bimberg, V. M. Ustinov, A. Y. Egorov, A. E. Zhukov, P. S. Kop'ev, S. V. Zaitsev, N. Y.

Gordeev, Z. I. Alferov, A. I. Borovkov, A. O. Kosogov, S. S. Ruvimov, P. Werner, U. Gosele, and J. Heydenreich, Phys. Rev. B 54, 12, 8743-8750 (1996).

[4] L. Bouzaiene, B. Ilahi, L. Sfaxi, F. Hassen, H. Maaref, O. Marty, and J. Dazord, Appl. Phys. A 79, 587-591 (2004).

[5] J. Lee, T. W. Saucer, A. J. Martin, J. Millunchick, and V. Sih, Phys. Rev. Lett. 110, 013602 (2013).

[6] V. Celibert, E. Tranvouez, G. Guillot, C. Bru-Chevallier, L. Grenouillet, P. Duvaut, P. Gilet, P. Ballet, and A. Million, J. of Cryst. Grth. 275, e2313-e2319 (2005).

[7] D. Englund, D. Fattal, E. Waks, G. Solomon, B. Zhang, T. Nakaoka, Y. Arakawa, Y. Yamamoto, and J. Vuckovic, Phys. Rev. Lett. 95, 013904 (2005).

[8] A. Badolato, K. Hennessy, M. Atature, J. Dreiser, E. Hu, P. M. Petroff, and A. Imamoglu, Science 308, 1158 (2005).

[9] J. Y. Lee, M. J. Noordhoek, P. Smereka, H. McKay, and J. M. Millunchick, Nanotechnology 20, No. 285305 (2009).

[10] A. J. Martin, T. W. Saucer, G. V. Rodriguez, V. Sih, and J. Millunchick, Nanotechnology 23**,** 135401 (2012).

[11] J. Lee, T. W. Saucer, A. J. Martin, D. Tien, J. M. Millunchick, and V. Sih, Nano Lett. 11, 1040-1043 (2011).

[12] J. Lee, T. W. Saucer, A. J. Martin, D. Tien, J. M. Millunchick, and V. Sih, J. of Luminescence 133, 117-120 (2013).

[13] T. W. Saucer, J. Lee, A. J. Martin, D. Tien, J. M. Millunchick, and V. Sih, Solid State Commun. 151, 269–271 (2011).

[14] M. Mehta, D. Reuter, A. Melnikov, A. D. Wieck, and A. Remhof, App. Phys. Lett. 91, 123108 (2007).

[15] J. M. Ulloa, R. Gargallo-Caballero, M. Bozkurt, M. del Moral, A. Guzman, P. M. Koenraad, and A. Hierro, Phys. Rev. B 81, 165305 (2010).

[16] J. M. Ulloa, I. W. D. Drouzas, P. M. Koenraad, D. J. Mowbray, M. J. Steer, H. Y. Liu, and M. Hopkinson, Appl. Phys. Lett. 90, 213105 (2007).

[17] J. G. Keizer, P. M. Koenraad, P. Smereka, J. M. Ulloa, A. Guzman, and A. Hierro, Phys. Rev. B 85, 155326 (2012).

[18] T. P. Schulze and P. Smereka, Phys. Rev. B 86, 235313 (2012).

[19] P. Offermans, P. M. Koenraad, J. H. Wolter, D. Granados, J. M. Garcia, V. M. Fomin, V. N. Gladilin, and J. T. DeVreese, Physica E 32, 41-45 (2006).

[20] H. S. Ling and C. P. Lee, J. of Appl. Phys. 102, 024314 (2007).

[21] L. Cuadra, A. Marti, and A. Luque *Physica E* **14** 162 (2002).

[22] I. Sukhoivanov and I. Guryev "Photonic Crystals: Physics and Practice Modeling", Springer, Verlag, Berlin, Heidelberg (2009).

[23] M. Luengo-Kovac, T. W. Saucer, A. J. Martin, J. Millunchick, V. Sih, *JVST B* in print, JVSTB-A-13-102 (2013).

PART II

Analysis of the Growth, Structure, and Optoelectronic Properties of GaSb Quantum Dots

Part II contains Chapters 5, 6, and 7, which present studies on GaSb/GaAs QDs that are of interest for photovoltaic applications because of their type-II band alignment. *The goal of Part II* is to provide an understanding of the effects of growth and capping conditions on the size, shape, and dissolution of GaSb QDs. Chapter 5 analyzes Sb segregation in quantum dot and well nanostructures using three-dimensional atom probe tomography and photoluminescence. Chapter 6 discusses the effects of surface reconstruction on QD dimensions and their physical and optical properties. Chapter 7 provides a more complete understanding of GaSb dot dissolution up capping by combining cross-sectional scanning tunneling microscopy with atom probe tomography to more accurately interpret GaSb QD photoluminescence. The findings presented in these chapters are used to effectively implement GaSb QDs into intermediate band solar cells in collaboration with Prof. Jamie Phillips' group in the Electrical Engineering department. Results from intermediate band solar cells, which were jointly fabricated with collaborators are also briefly discussed.

Chapter 5

Atom Probe Tomography Analysis of Different Modes of Sb Intermixing in GaSb Quantum Dots and Wells

Different modes of intermixing are observed in GaSb/GaAs layers via atom probe tomography. The intermixing length scale for quantum wells of varying thickness is on the order of a monolayer, but three times longer for the wetting layer of a quantum dot structure. The former arises from segregation of Sb and/or surface-induced intermixing via detachment from step edges. The latter is dominated by surface-induced intermixing due to disintegration of the GaSb dots upon capping.

5.1 Introduction

The type-II band alignment of GaSb/GaAs quantum dots (QDs) makes them of particular interest for a number of semiconductor device applications including intermediate band solar cells[1-4] and charge storage devices.[5] While their optical properties,[6-8] and morphological and compositional changes upon capping[9-16] have received a great deal of attention, the two- to three-dimensional transition during GaSb QD nucleation has not been well studied.[8] It is well known that in the Stranski-Krastanov growth mode QDs nucleate after some critical film thickness is surpassed[17] in an effort to relax strain.[8] During this two- to three-dimensional transition, QDs form as a result of mass transfer from the initially deposited thin film to the dots[8] with a wetting layer of some thickness remaining between the dots. Intermixing during subsequent capping of

the nanostructures can affect the structure and composition of both the two-dimensional layer and the QDs, although perhaps not in the same manner. Understanding intermixing is important because the dissolution of buried structures can significantly affect their optoelectronic properties[16,18] and, subsequently, any semiconductor devices into which they are implemented.

It is well known that Sb readily segregates, particularly in GaSb QD nanostructures where the morphology of the dots can be significantly altered during GaAs capping.[9-16] Recent studies have relied primarily on two-dimensional analytical techniques[8,11,12,15] such as transmission electron microscopy and cross-sectional scanning tunneling microscopy to investigate changes to the morphology and composition of buried nanostructures. Atom probe tomography possesses a unique ability to look at concentrations within buried nanostructures in three dimensions with atomic resolution, making it uniquely suited for this type of analysis.[16,19,20] The goal of this chapter is to use atom probe tomography coupled with photoluminescence to investigate the different modes of intermixing observed in two- and three-dimensional GaSb nanostructures in order to better understand the changes in film composition that occur during QD nucleation and capping.

5.2 Experimental Procedure

Multilayer GaSb/GaAs samples with varying GaSb thickness were grown by molecular beam epitaxy on GaAs(001) substrates. For each sample, a 500 nm GaAs buffer layer was grown at a rate of 1.0 monolayer (ML) s^{-1}. Samples were cooled to T = 460 ^{o}C, as measured by an optical pyrometer, for deposition of 1.0, 1.5, and 2.3 ML of GaSb at a rate of 0.3 MLs^{-1} and a V/III ratio of 2, immediately followed by a GaAs spacer layer of 10 nm for the 1.0 and 1.5 ML samples and 20 nm for the 2.3 ML sample grown at the same rate as the GaSb layers. Photoluminescence (PL) measurements were taken at T = 10 K in a helium flow cryostat at 525

μW using a HeNe laser operating at 633 nm. The PL spectrum was collected using a 0.75 m spectrometer with a 150 G/mm reflection grating and a single channel InGaAs detector.

The samples were prepared for atom probe tomography (APT) using a standard focused ion beam lift-out technique[21] and annularly milled to a tip diameter of less than 100 nm at the apex. Analysis was done in a Cameca LEAP 4000X operated at 20 K in laser pulsing mode with a laser energy of 0.25 pJ. APT analysis for the 2.3 ML GaSb sample was done on a separate sample grown under the same conditions as the first (*i.e.*, same growth rates, temperatures, and amount of GaSb deposited), however, the sample consisted of five GaSb layers and had a 50 nm spacer. Reconstruction parameters (*i.e.*, image compression factor and the value of the evaporation field) were selected to yield flat GaSb layers with the correct layer spacing. All samples were reconstructed using the same evaporation field, and only minor variations to the image correction factor were made to ensure flat GaSb layers.

5.3 Data Analysis

5.3.1 Photoluminescence of Quantum Dot and Well Structures

Analysis of the PL with respect to increasing GaSb thickness provides insight into the structural and compositional changes that occur during the two- to three-dimensional transition that takes place when QDs nucleate. PL spectra for the 1.0 and 1.5 ML quantum wells and 2.3 ML QD samples are shown in Figure 5.1. As the quantum well thickness increases from 1.0 to 1.5 ML of GaSb, the PL peak energy shifts from 1.37 to 1.26 eV as expected for an increase in quantum well thickness. The full width at half maximum also increases from 30 to 86 meV for the 1.0 and 1.5 ML samples, respectively, which likely results from a decrease in the uniformity of the film thickness for the 1.5 ML sample. For the 2.3 ML sample, the film thickness surpasses

the critical thickness for QD nucleation, resulting in a QD PL peak centered around 1.15 eV. Rather than continuing to shift to lower energy, the wetting layer peak blue shifts to 1.36 eV and has a full width at half maximum of 80 meV. The presence of the wetting layer peak at 1.36 eV indicates a decrease in thickness and/or change in composition as a result of QD nucleation. Additionally, the linewidth of 80 meV is likely the result of a non-uniform wetting layer thickness and/or concentration.

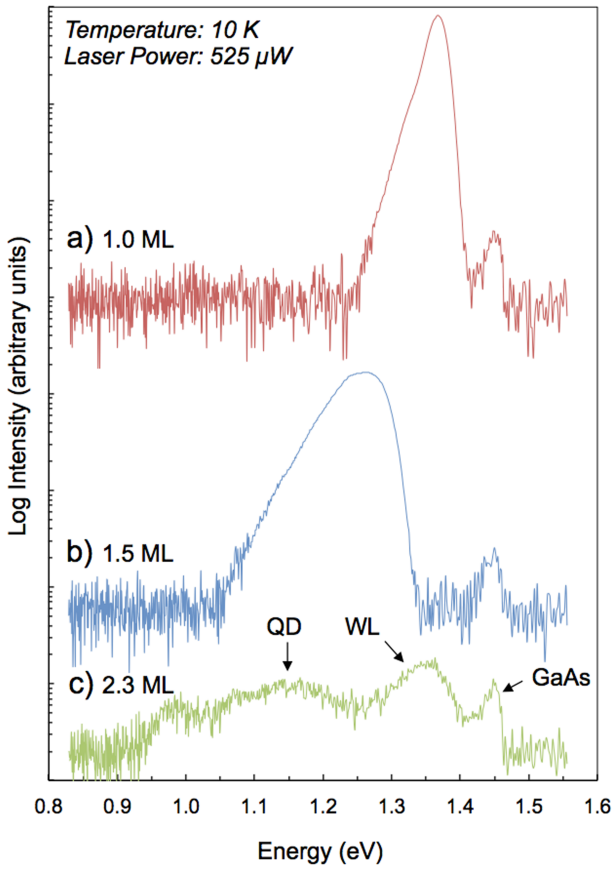

Figure 5.1: Photoluminescence spectra from (a) a 1.0 ML GaSb quantum well, (b) a 1.5 ML GaSb quantum well, and (c) a 2.3 ML GaSb QD structure showing QD emission at 1.15 eV and a wetting layer peak at 1.36 eV. All intensities are normalized to the GaAs peak intensity, which is at approximately 1.45 eV. Photoluminescence specta collected by Timothy W. Saucer and Garrett V. Rodriguez, Prof. Vanessa Sih group, Physics.

5.3.2 Sb Concentration Profiles for Buried Nanostructures

Atom probe tomography has the ability to measure compositional changes within the buried nanostructures and provide information about Sb segregation within the different nanostructures. Figure 5.2 shows three-dimensional APT reconstructions of the 1.0 and 1.5 ML GaSb quantum well samples with Sb atoms highlighted in blue. A profile of the Sb concentration as a function of position is shown beside each multi-layer structure. Sb concentration profiles were measured using a 10 nm diameter cylinder aligned down the center of the three-dimensional reconstruction and perpendicular to the layers. A bin size of 0.2 nm was used because it is nominally the same size as the atoms within the structure.

The average Sb concentration profile of each quantum well sample and that of the wetting layer in the 2.3 ML QD sample are compared in Figure 5.3. The average Sb concentration profiles for both quantum well samples were taken only from the middle six layers because the data was reconstructed to ensure that the center layers of the sample were the flattest. Sb concentration profiles for the wetting layer in the 2.3 ML sample were taken at multiple locations within the sample and away from the edges of the reconstruction. No correlation was seen in the Sb concentration profile with respect to the relative distance from a QD. For each sample, the interface between the GaSb and the underlying GaAs is not atomically abrupt. This effect has been considered by others to arise due to the effect of averaging of several volumes when determining the Sb concentration for each bin in the z direction.[19] The shape of the interface could also be due to surface roughness of the underlying GaAs and/or a small amount of downward intermixing of Sb.[16,22]

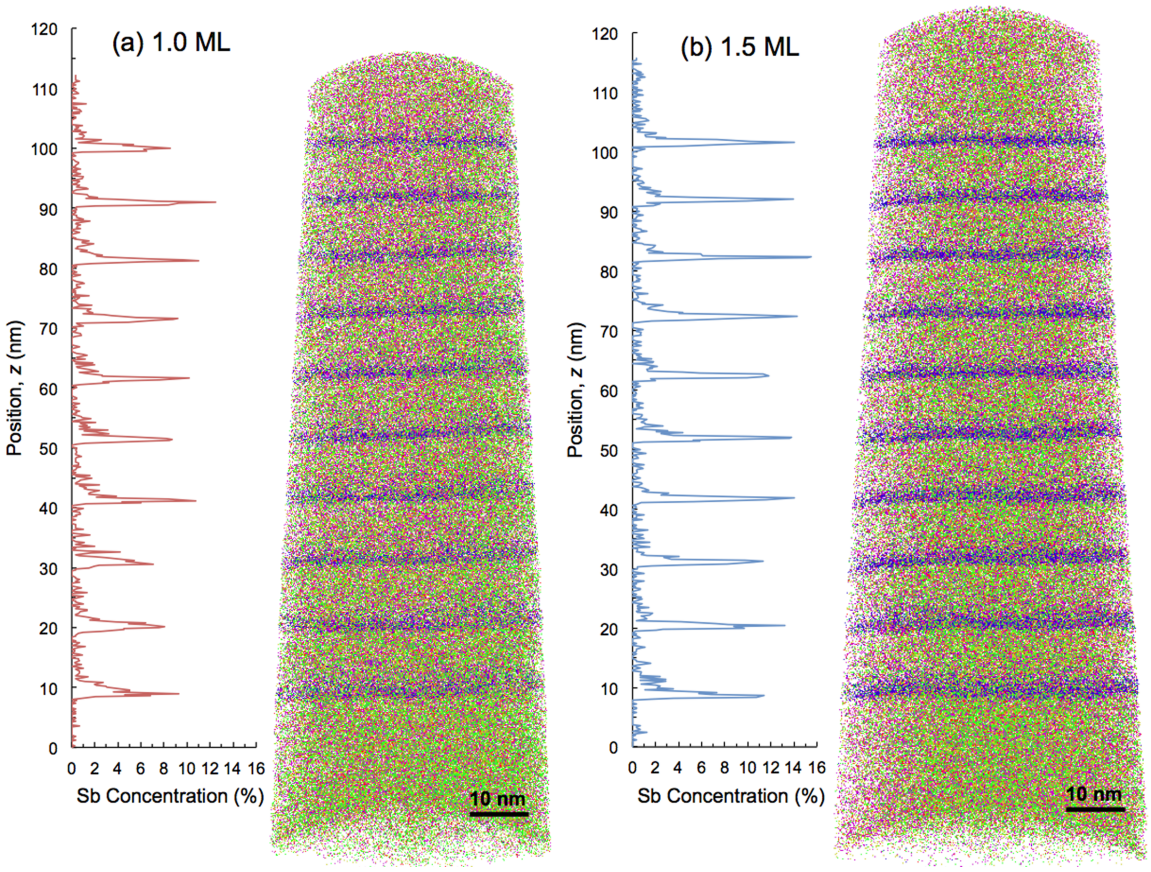

Figure 5.2: Three-dimensional reconstructions of atom probe tomography data for (a) a 1.0 ML quantum well and (b) a 1.5 ML GaSb quantum well. The Sb atoms are shown in blue. The Sb concentration profile for each structure is shown to the left of the three-dimensional reconstruction. Sb concentration profiles are taken from a 10 nm cylinder with a 0.2 nm bin size through the center of the structures, perpendicular to the GaSb layers. APT data collected by Dr. Allen H. Hunter, Prof. Emmanuelle Marquis group, MSE.

The Sb concentration for the 1.5 ML sample peaks at approximately 50% greater than that of the 1.0 ML sample, which is expected because there is 50% more Sb in the 1.5 ML quantum well sample. The Sb concentration profile is also broader in the *z* direction for the 1.5 ML sample due to the greater deposited film thickness. Rather than continuing to increase beyond the Sb concentration of the 1.5 ML sample, the Sb concentration in the wetting layer of

the 2.3 ML sample peaks at approximately the same concentration as the 1.0 ML quantum well. Based on the PL data alone, this is expected because the emission energy of the wetting layer peak for the 2.3 ML sample is approximately the same as that of the 1.0 ML quantum well. However, the Sb concentration profile for the wetting layer is very different than that of either quantum well sample, having higher Sb concentrations observed at larger *z* values.

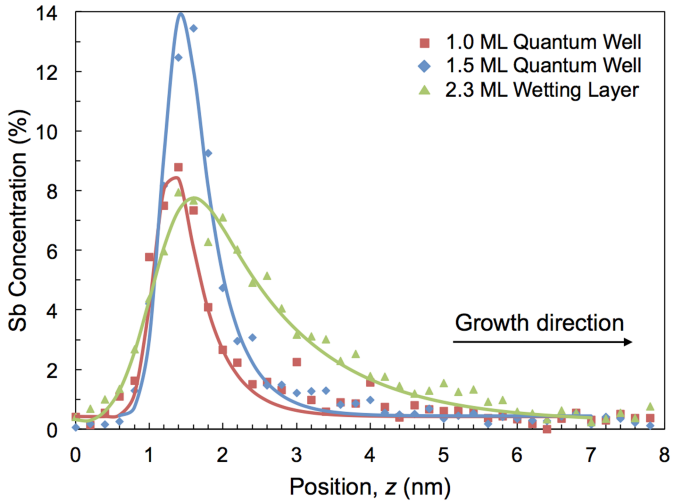

Figure 5.3: Sb concentration profiles for the 1.0 ML and 1.5 ML quantum wells and the wetting layer in the 2.3 ML QD sample. All Sb concentration profiles are taken using a 10 nm diameter area and a bin size of 0.2 nm, perpendicular to the GaSb layers. Solid lines are fits to the Sb concentration profiles.

The number of Sb atoms per unit volume can be summed from the atom probe data for each structure and compared to the number of deposited Sb atoms for that given volume. The number of summed Sb atoms for each structure is adjusted based on the detection efficiency of the atom probe, which is defined by Cameca to be 36% for the Cameca LEAP 4000X used in these experiments. After making this adjustment, the expected number of Sb atoms within a 10 nm diameter area for the 1.0, 1.5, and 2.3 ML samples is approximately 152, 228, and 350, respectively. We find that the average number of Sb atoms summed from the APT data for the

1.0 and 1.5 ML quantum wells and the wetting layer of the 2.3 ML sample are 196 ± 14, 259 ± 21, and 377 ± 76, respectively, which are consistently slightly higher than expected, perhaps the result of the shutter actuation time of the Ga and Sb shutters. The summed number of Sb atoms in the quantum wells is expected to closely match the deposited number. The summed number of Sb atoms in the wetting layer, on the other hand, should be less than the deposited number due to dot nucleation. The additional Sb in the wetting layer likely arises from the disintegration of the QDs upon capping,[16] and it intermixes with the arriving GaAs during capping. The large standard deviation in the number of Sb atoms in the wetting layer demonstrates its non-uniform thickness, and a larger sample size would likely show some locations with significantly less Sb.

5.3.3 Analysis of Different Modes of Sb Intermixing

The Sb concentration profiles can be modeled by convolution of a Gaussian distribution representing the deposited GaSb layer and an exponential decay representing the intermixing.[19] Table I shows the fitting parameters for each type of structure. The 1.0 and 1.5 ML profiles can both be characterized as having a Gaussian distribution of atoms with a width of 0.3 nm convoluted with an exponential decay in the growth direction having a length scale of 0.4 nm, which are both on the order of a ML. The two profiles only differ in the amplitude of the Gaussian (the concentration of Sb in the layer), as expected. The wetting layer of the 2.3 ML sample has an amplitude similar to that of the 1.0 ML quantum well, consistent with the PL data. The layer width is 0.4 nm, similar to the quantum wells, but the exponential decay length is 1.3 nm.

The fact that the Sb decay length scales are different in the wetting layer of the 2.3 ML sample compared to both quantum wells suggests that they have different mechanisms for

intermixing during GaAs capping. The short decay length scale is likely due to Sb segregation, which results when Sb atoms within the GaSb layer exchange with surface As atoms during capping. The length scale of such a mechanism would be expected to be on the order of a ML or two, in agreement with the observed data. The longer decay length scale results as a consequence of surface intermixing where Sb atoms detach from step edges or come from disintegrating QDs, allowing them to become intermingled with As atoms during capping. The fact that the length scale of surface-induced intermixing is approximately three times longer than that of Sb segregation is consistent with the expectation that it is a lower energy process. That is, the energy to detach a relatively low-coordinated atom from a step edge is less than the energy to remove a higher-coordinated atom from within the layer. It is likely that both Sb segregation and surface intermixing processes occur during capping. In the 2.3 ML sample, however, QD dissolution provides a large source of Sb that can intermix, overwhelming Sb segregation in this case.

Table I: Fits for Sb Concentration Profiles

Structure	Gaussian Prefactor (arb. units)	Width (nm)	Decay Length Scale (nm)
1.0 ML WL	0.35	0.3	0.4
1.5 ML WL	0.55	0.3	0.4
WL from 2.3 ML	0.30	0.4	1.3
Cluster from 2.3 ML	1.5	1.2	0.4
QD from 2.3 ML	3.5	2.0	0.4

The Sb concentration profile of the wetting layer in the 2.3 ML sample can also be compared to the profile through a compact QD and a cluster of small islands. Figure 5.4 (a) shows a three-dimensional reconstruction from the 2.3 ML sample analyzed by APT. Sb atoms are shown in blue and a 14% Sb iso-concentration surface is highlighted in yellow showing one compact QD and one cluster of small islands. Figure 5.4 (b) shows the Sb concentration profile through the compact QD, the islands within the cluster, and wetting layer. Data for the QD is collected using a 10 nm diameter area with a bin size of 0.2 nm in the *z* direction. For the cluster,

a 4 nm diameter area and bin size of 0.2 nm in *z* are used to analyze the Sb concentration profile through only the small islands of the cluster, not including the Sb-void center. The inset in Figure 5.4 (b) shows a top-down view of the nanostructures observed in this particular APT volume and, again, a 14% Sb iso-concentration surface is highlighted in yellow. The Sb concentration in the QD reaches over 35% and decreases rapidly above the dot with a similar decay profile to both quantum well samples. The cluster follows a similar trend, but only reaches a peak Sb concentration of approximately 25% through the small islands and is significantly less broad in *z*. The amplitude of the Gaussians for the QD and the cluster are 3.5 and 1.5, respectively, due to their higher Sb concentrations. The length scale of the exponential decay for both the QD and cluster is 0.4 nm (Table I), which is the same as that of the quantum wells. Therefore, these structures are also dominated by segregation during capping. Surface intermixing is not significant above the dot and cluster because Sb is actively diffusing away from the nanostructures to wet the surrounding GaAs during capping.[24-26] Therefore, these structures are also dominated by segregation during capping.

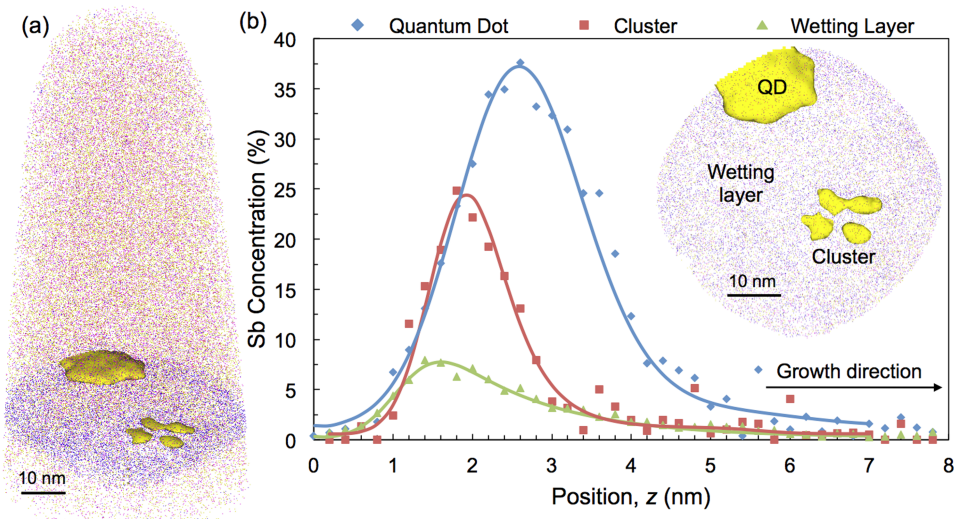

Figure 5.4: (a) A three-dimensional reconstruction of atom probe tomography data from the 2.3 ML QD sample showing one compact QD and one disintegrated cluster of smaller islands with a 14% Sb concentration surface highlighted in yellow. (b) Sb concentration profiles through the QD, cluster, and wetting layer. The profiles for the QD and wetting layer were taken using a 10 nm diameter area and a bin size of 0.2 nm, perpendicular to the GaSb layer. The profile for the cluster was taken using a 4 nm diameter only through the small GaSb islands. Solid lines are fits to the Sb concentration profiles. The inset shows a top-down view of the GaSb nanostructures analyzed. APT data collected by Prof. Emmanuelle Marquis, MSE.

5.4 Conclusions

In conclusion, different modes of intermixing are observed in buried two- and three-dimensional GaSb nanostructures using atom probe tomography. Two modes of Sb intermixing during capping are evident by differences in the Sb concentration profiles of these structures. These two modes are segregation and surface-induced intermixing, which have length scales of approximately 0.4 and 1.3 nm, respectively. A higher density of step edges and disintegration of GaSb QDs during capping introduces excess Sb in the QD sample, causing surface intermixing

to dominate the Sb concentration profile of the wetting layer. The Sb concentration profiles for the compact QD and disintegrated cluster of small islands are consistent with those seen in the quantum well structures.

5.5 References

[1] A. Luque and A. Marti, Phys. Rev. Lett. **78(26)** 5014 (1997).

[2] A. Marti, L. Cuadra, and A. Luque, Proceedings of the 28th IEE Photovoltaics Specialists Conference (IEEE, New York, 2000), p. 940.

[3] L. Cuadra, A. Marti, and A. Luque, Physica E **14** 162 (2002).

[4] A. Marti, N. Lopez, E. Antolin, E. Canovas, C. Stanley, C. Farmer, L. Cuadra, and A. Luque Thin Solid Films **511–512** 638–644 (2006).

[5] M. Geller, C. Kapteyn, L. Muller-Kirsch, R. Heitz, and D. Bimberg, Appl. Phys. Lett. **82(16)** 2706–2708 (2003).

[6] F. Hatami, M. Grundmann, N. N. Ledentsov, F. Heinrichsdorff, R. Heitz, J. Bohrer, D Bimberg, S. S. Ruvimov, P. Werner, V. M. Ustinov, P. S. Kop'ev, Zh. I. Alferov, Phys. Rev. B **57**,**8** 4635-4641 (1998).

[7] G. Balakrishnan, J. Tatebayashi, A. Khoshakhlagh, S. H. Huang, A. Jallipalli, L. R. Dawson, and D. L. Huffaker, Appl. Phys. Lett. **89** 161104 (2006).

[8] L. Muller-Kirsch, R. Heitz, U. W. Pohl, and D. Bimberg, Appl. Phys. Lett. **79, 7** 1027-1029 (2001).

[9] R. Timm, H. Eisele, A. Lenz, L. Ivanova, G. Balakrishnan, D. L. Huffaker, and M. Dahne, Phys. Rev. Lett. **101** 256101 (2008).

[10] R. Timm, A. Lenz, H. Eisele, L. Ivanova, G. Balakrishnan, D.L. Huffaker, I. Farrer, D. A. Ritchie, and M. Dahne, J. of Vac. Sci. & Tech. B **26(4)** 1492 (2008).

[11] R. Timm, H. Eisele, A. Lenz, L. Ivanova, V. Vosseburger, T. Warming, D. Bimberg, I. Farrer, D. A. Ritchie, and M. Dahne, Nano Lett. **10** 3972 (2010).

[12] E. P. Smakman, J. K. Garleff, R. J. Young, M. Hayne, P. Rambabu, and P. M. Koenraad, Appl. Phys. Lett. **100** 142116 (2012).

[13] R. J. Young, E. P. Smakman, A. M. Sanchez, P. Hodgson, P. M. Koenraad, and M. Hayne, Appl. Phys. Lett. **100** 082104 (2012).

[14] A. M. Beltran, E. A. Marquis, A. G. Taboada, J. M. Ripalda, J. M. Garcia, and S. I. Molina, Ultramicroscopy **111** 1073 (2011).

[15] M.A. Kamarudin, M. Hayne, R. J. Yound, Q. D. Zhuang, T. Ben, and S. I. Molina, Phys. Rev. B **83** 115311 (2011).

[16] A. J. Martin, J. Hwang, E. A. Marquis, E. P. Smakman, T. W. Saucer, G. V. Rodriguez, A. H. Hunter, V. Sih, P. M. Koenraad, J. D. Phillips, and J. Millunchick Appl. Phys. Lett. **102** 113103 (2013).

[17] K. Suzuki, R. A. Hogg, K. Tachibana, and Y. Arakawa Jpn. J. Appl. Phys. **37** L203-L205 (1998).

[18] M. Bozkurt, J. M. Ulloa, and P. M. Koenraad Semicond. Sci. Technol. **26** 064007 (2011).

[19] A. D. Giddings, J. G. Keizer, M. Hara, G. J. Hamhuis, H. Yuasa, H. Fukuzawa, and P. M. Koenraad, Phys. Rev. B **83** 205308 (2011).

[20] M. Muller, A. Cerezo, G. D. W. Smith, L. Chang, and S. S. A. Gerstl Appl. Phys. Lett. **92** 233115 (2008).

[21] K. Thompson, D. Lawrence, D. J. Larson, J. D. Olson, T. F. Kelly, and B. Gorman, Ultramicroscopy **107** 131 (2007).

[22] Ch. Heyn, A. Schramm, T. Kipp, and W. Hansen J. of Cryst. Gr. **301-302** 692-696 (2007).

[23] P. Offermans, P. M. Koenraad, R. Notzel, J. H. Wolter, and K. Pierz, Appl. Phys. Lett. **87** 111903 (2005).

[24] J. G. Keizer, P. M. Koenraad, P. Smereka, J. M. Ulloa, A. Guzman, and A. Hierro, Phys. Rev. B **85** 155326 (2012).

[25] T. P. Schulze and P. Smereka, Phys. Rev. B **86** 235313 (2012).

[26] A. J. Martin, T. W. Saucer, V. Sih, and J. Millunchick Appl. Phys. Lett. **102** 182105 (2013).

Chapter 6

Analysis of Defect-Free GaSb/GaAs(001) Quantum Dots Grown on the Sb-terminated (2x8) Surface

Multilayer and single layer GaSb/GaAs(001) quantum dot structures were grown on an Sb-terminated (2x8) surface reconstruction and compared to those grown on an As-terminated (2x4) surface reconstruction. Uncapped quantum dots grown on the (2x8) surface were approximately 25% smaller in diameter and had a larger width/height aspect ratio. Quantum dots grown on both surfaces were defect free at the quantum dot/spacer layer interface. The dots did not appear to be fully compact when imaged by transmission electron microscopy, which may be due to dissolution and/or quantum ring formation. The quantum dot photoluminescence peak for dots grown on the (2x8) surface was brighter but at the same energy as that of dots grown on the (2x4) surface. This was likely the result of a higher areal density of dots on the (2x8) surface and a lower tendency for them to intermix during capping, resulting in dots of similar size for both samples after capping. Quantum dots grown on the (2x8) surface also displayed greater morphological stability when quenched in the absence of Sb.

6.1 Introduction

Quantum dots (QD) are of recent interest for use in photovoltaics,[1-4] charge storage devices,[5] and lasers.[6,7] Particularly, GaSb/GaAs QDs are of interest for intermediate band solar cells because of their type-II band offset, which is believed to reduce random recombination and

increase charge separation and carrier lifetime.[3] Densely packed QDs and QD stacking are desirable for increasing absorption in solar cell applications, and quantum dot morphology affects the electronic properties of the dots. However, much remains to be understood about the effects of altering growth conditions on these properties in order to implement GaSb QDs in high-efficiency intermediate band solar cells. For example, changes in QD morphology and Sb-As exchange that often occur during capping can negatively alter the optical and electronic properties of the resulting dots. One particular growth condition that affects these specific properties is the starting surface reconstruction on which the QDs are grown. The starting surface reconstruction has been shown to affect the areal density, size, shape, defect structure, and photoluminescence emission energy of the resulting QDs when comparing dots grown on the As-terminated (2x4) and Sb-terminated (2x8) surfaces.[8,9] This chapter analyzes multilayer and single layer GaSb/GaAs(001) QD structures grown on the (2x4) and (2x8) surfaces, comparing the resulting microstructure and optical properties.

6.2 Experimental Procedure

Multilayer and single layer GaSb/GaAs(001) QD structures were grown by molecular beam epitaxy on the As-terminated (2x4) and Sb-terminated (2x8) surface reconstructions, for a total of four samples. Figure 1 shows reflective high energy electron diffraction patterns along [$\bar{1}$10] for the two surfaces. All samples had a 500 nm GaAs buffer layer grown at T = 590 ^{o}C. The QD growth temperature for all samples was T = 460 ^{o}C. All temperatures reported were measured using an optical pyrometer. QDs were grown at a rate of 0.3 monolayers (ML) per second with a V/III ratio of 2.0. The multilayer samples were immediately capped with a 20 nm GaAs spacer layer at a rate of 0.3 MLs^{-1} for each QD layer, and consisted of a total of 11 layers of QDs. The spacer layer thickness of 20 nm is nearly three times the thickness required for 90-

100% strain correlation between QD layers.[10,11] Therefore, the size and position of QDs at each layer was not expected to effect that of subsequent layers of dots. The QDs on the topmost surface of all samples remained uncapped for analysis by atomic force microscopy (AFM). The single layer samples were quenched under no group V overpressure in order to compare the morphological stability of dots grown on each surface reconstruction in the absence of Sb.

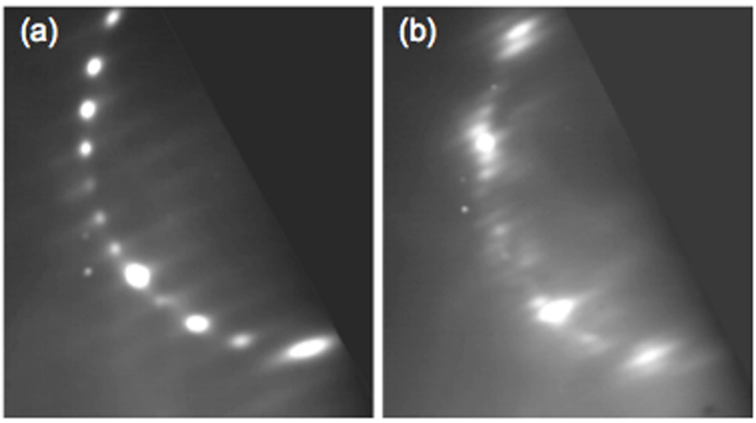

Figure 6.1: Reflective high energy electron diffraction patterns along [$\bar{1}$10] for (a) the As-terminated (2x4) surface reconstruction and (b) the Sb-terminated (2x8) surface reconstruction.

The As-terminated (2x4) surface reconstruction (Figure 6.1 (a)) was the reconstruction present after GaAs buffer growth. 2.3 ML of GaSb was deposited for QDs in the (2x4) multilayer and single layer samples. The Sb-terminated surface reconstruction (Figure 6.1 (b)) was achieved by increasing the temperature to T = 580 ^{o}C and exposing the surface to an Sb flux of 0.6 MLs^{-1}. Upon exposing the surface to Sb, the sample was immediately cooled under Sb flux at a rate of 30 ^{o}C/min to T = 460 ^{o}C for QD growth. The surface reconstruction changed to the Sb-terminated (2x8) during cooling to the QD growth temperature.[12,13] Formation of the Sb-terminated (2x8) surface essentially created a ~1.0 ML GaSb wetting layer on the surface due to Sb-As exchange, allowing Sb to bond to the underlying Ga as As left the surface. An additional

1.0 ML of GaSb was deposited at T = 460 ^{o}C for a total thickness of ~2.0 ML, subsequently forming QDs. For the multilayer sample, the (2x8) surface was achieved by this method for each layer prior to QD growth.

6.3 Data Analysis

6.3.1 Differences in QD Dimensions and Areal Density

AFM analysis of the uncapped surface QDs of the multilayer samples showed that dots grown on the As-terminated (2x4) surface were 25% larger in diameter and 50% larger in height than QDs grown on the Sb-terminated (2x8) surface. Figure 6.2 shows AFM images of the uncapped 11th layer of QDs for both multilayer samples. The average QD diameter and height for dots grown on the (2x4) surface were 42 ± 5 nm and 3.6 ± 0.9 nm, respectively. The average QD diameter and height for dots grown on the (2x8) surface were 34 ± 4 and 2.3 ± 0.7 nm, respectively. Although the difference in QD size for the two samples may be in part due to the small difference in the amount of GaSb deposited, the width/height aspect ratio of 12 ± 3 for the QDs grown on the (2x4) was smaller than 16 ± 3 for the QDs grown on the (2x8). Therefore, the QDs grown on the (2x8) surface were not only a different size, but also a different shape than those grown on the (2x4) surface.[8] Additionally, the areal density of QDs for the (2x4) and (2x8) multilayer samples were 3.5 x 10^{10} cm^{-2} and 5.3 x 10^{10} cm^{-2}, respectively, approximately 50% greater for the (2x8) multilayer sample. The areal densities measured were consistent with those reported in literature for GaSb QDs grown in a similar manner on the same starting surfaces.[8] The difference in dot density may have resulted from a faster QD nucleation rate on the (2x8) surface than on the (2x4) surface due to the differences in surface energy resulting from the different surface reconstructions. In either case, the surface reconstruction affected QD size,

shape, and areal density. Uncapped QD dimensions and the areal density were also measured on a single layer QD sample grown on the (2x8) surface and were not significantly different than those of the multilayer sample. Therefore, it is believed that the QD measurements from the multilayer samples are representative of each layer of QDs within the multilayer structures.

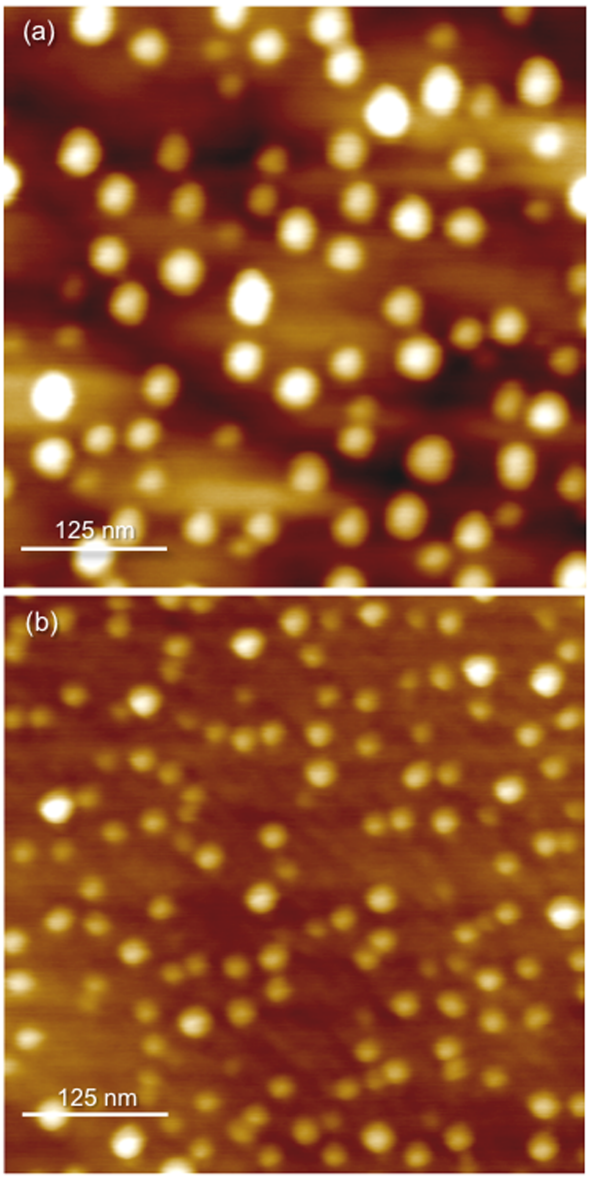

Figure 6.2: AFM images of the uncapped 11th layer of QDs grown on (a) the (2x4) surface and (b) the (2x8) surface showing the difference in QD size, shape, and areal density for dots grown on the different starting surface reconstructions. The height scale is 8 nm.

6.3.2 Analysis of Defect Free QD Structures

Transmission electron microscopy (TEM) was used to examine the QD/spacer layer interface. Figure 6.3 (a) and (c) show bright field TEM images of QDs from both samples. Figure 6.3 (b) and 3(d) show high resolution scanning TEM (STEM) images of the QD/spacer layer interface for both samples in high angle annular dark field (HAADF) mode. Many groups have reported the formation of ring-like structures upon GaAs capping of GaSb QDs.[14-17] In the bright field and HAADF images, it is difficult to determine if the QDs are in fact compact dots or ring-like structures due to the imaging technique. In TEM imaging, electrons are scattered through a finite volume of material, making it difficult to discern between the different types of nanostructures that have been reported. However, the HAADF images do clearly show the lattice, and a defect-free QD/spacer layer interface can be seen for both samples. Our observation of a defect-free QD/spacer layer interface in the (2x8) sample is in contrast to the results of Balakrishnan *et al.*, which showed an interfacial misfit dislocation array at the QD/spacer layer interface for dots grown on the Sb-terminated (2x8) surface.[8,9] The formation of a defect-free interface may be the result of achieving the (2x8) reconstruction via a different method than previously reported in literature[8,18] or due to the heating and cooling cycles we used to achieve the (2x8) for each layer prior to QD growth, which essentially acted as low temperature annealing stages. Nonetheless, this is a unique result for QDs grown on the Sb-terminated (2x8) surface.

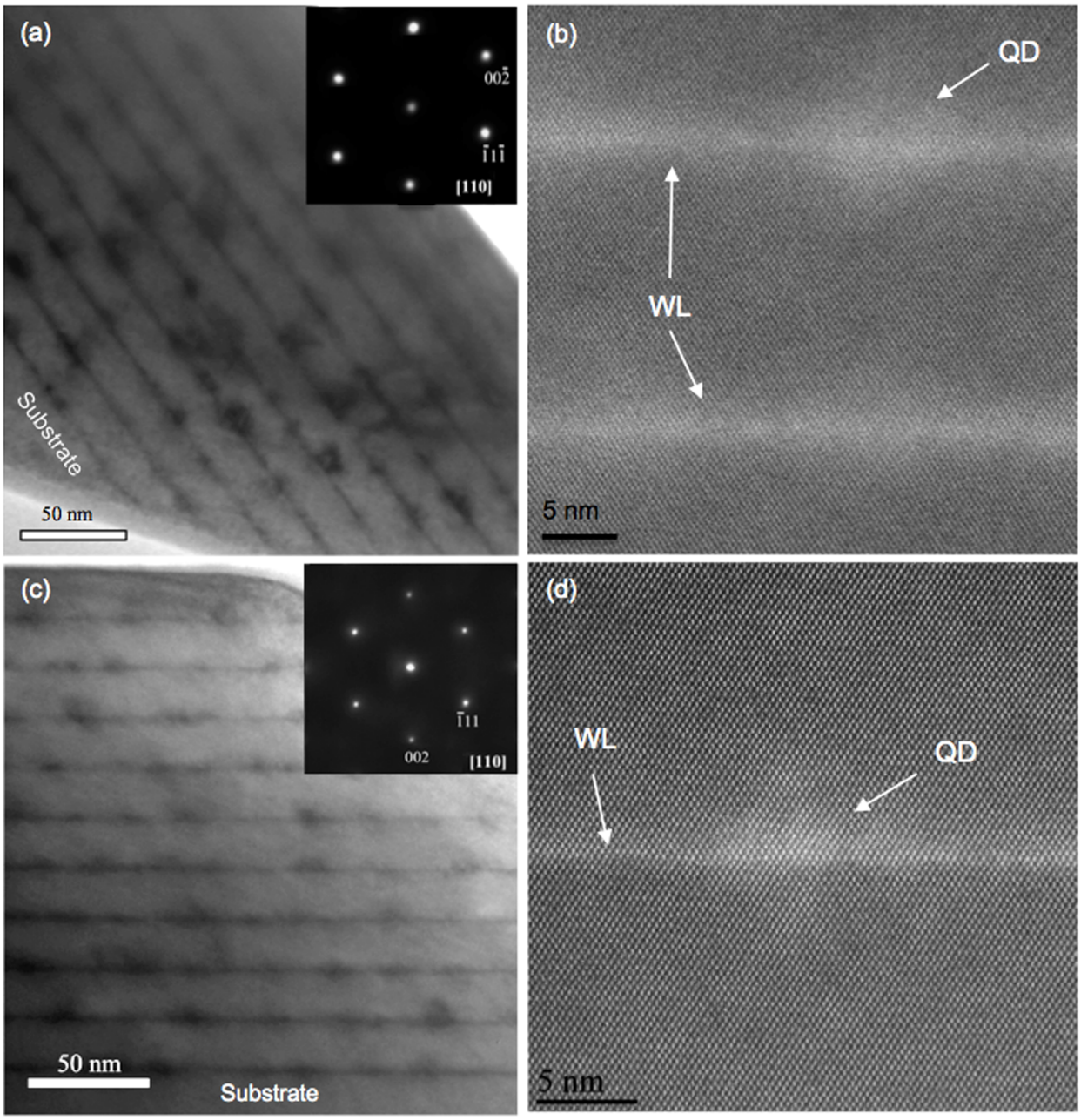

Figure 6.3: (a) and (b) Bright field TEM and high resolution HAADF images of QDs grown on the As-terminated (2x4) surface, respectively. (c) and (d) Bright field TEM and high resolution HAADF images of QDs grown on the Sb-terminated (2x8) surface, respectively. The HAADF images show a defect-free QD/spacer layer interface for both samples. Images taken by Dr. Guang Ran, Prof. Lumin Wang group, and Sung Joo Kim, Prof. Xiaoqing Pan group, MSE Department.

6.3.3 QD Photoluminescence Properties

Both multilayer samples displayed similar optical properties. Figure 6.4 shows the photoluminescence (PL) spectra for both multilayer samples. PL measurements were taken at 10 K in a helium flow cryostat at 424.5 and 362.5 μW for the (2x4) and (2x8) samples, respectively, using a HeNe laser operating at 633 nm. The spectra were collected using a 0.75 m spectrometer with a 150 G/mm reflection grating and a single channel InGaAs detector. The GaAs substrate peak is at 1.48 eV. The wetting layer (WL) peak is at 1.35 eV. There is a split QD peak at 1.13 and 1.18 eV.[19-21] Hatami *et al.* attributed this double peak to the QD and WL because the intensity of the higher energy peak dropped off more rapidly with temperature than the lower energy peak in a similar fashion to the WL peak in an InAs/GaAs system.[19] However, the intensity versus temperature trend for our samples is inconsistent with these results. The split peak may be attributed to a bimodal QD size distribution; however, AFM of the uncapped QDs did not show a bimodal distribution. Instead, the split peak may the result of QD dissolution and quantum ring formation upon capping.[14-16] The PL spectra are consistent with those shown from GaSb/GaAs quantum rings.[17] There were also two low energy peaks at 0.97 and 1.07 eV, which we attribute to exciton emission because their peak intensities increase linearly with increasing laser power. The peak positions were the same for both samples, but the intensity of the QD peak for the (2x8) sample is greater with respect to the GaAs peak than that of the (2x4) sample. This is most likely a result of the higher density of QDs on the (2x8) surface. Consistent with these results, the WL peak intensity is weaker for the (2x8) sample.

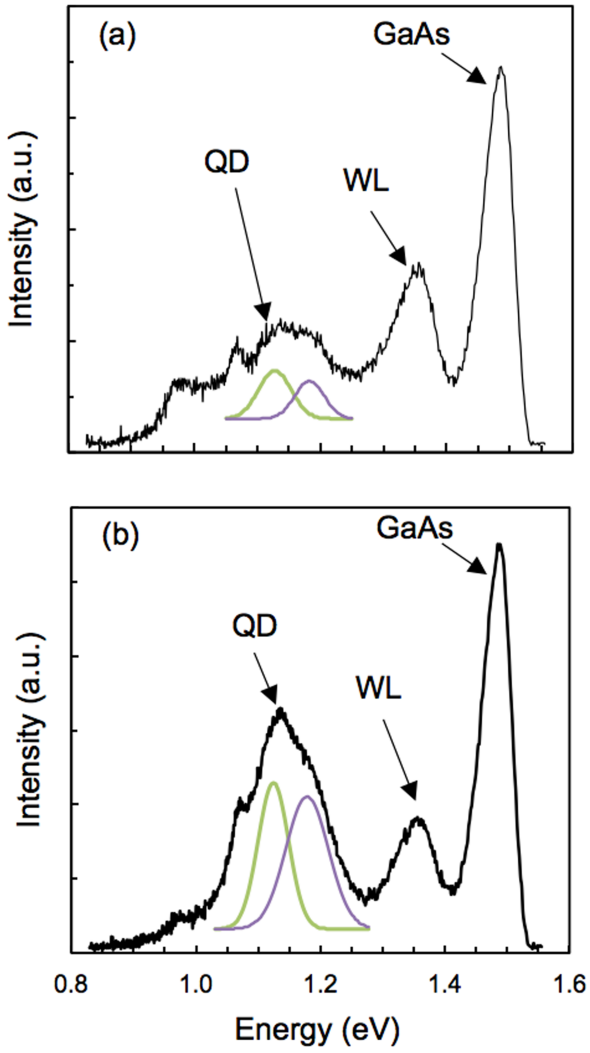

Figure 6.4: PL spectra taken at 10 K for the multilayer samples grown on (a) the (2x4) surface and (b) the (2x8) surface. The GaAs peak is at 1.48 eV and the WL peak is at 1.35 eV. There is a split QD peak is at 1.13 and 1.18eV, which may be due to quantum ring formation upon capping. There are also two low energy peaks at 0.97 and 1.07 eV, which we attribute to exciton emission. Gaussian peak fits are show for the QD (1.13 eV) and WL (1.18 eV) peaks. Data collected by Timothy W. Saucer and Garrett V. Rodriguez, Prof. Vanessa Sih group, Physics Department. Peak fitting program developed by Prof. Thomas O'Haver, University of Maryland.

6.3.4 Dissolution Dependence on Surface Reconstruction

The QD and WL peaks are at the same energies for both multilayer samples despite the difference in the size and shape of the uncapped surface QDs. Therefore, it is believed that the QDs grown on the As-terminated (2x4) surface dissociated more readily during capping than the dots grown on the Sb-terminated (2x8) surface, creating dots of similar sizes upon capping. This tendency to dissociate was verified by the growth of single layer, uncapped samples grown on each surface reconstruction, which were quenched under no group V overpressure. Figure 6.5 shows AFM images of these samples. In the absence of an Sb flux, QDs on the As-terminated (2x4) surface quickly dissociated as Sb left the surface, leaving only a remnant of the QDs behind as seen in Figure 6.5 (a). Close inspection of this image shows that the remnant structures are ring-like. In contrast, the QDs grown on the Sb-terminated (2x8) surface remained morphologically unchanged when quenched in the absence of Sb as seen in Figure 6.5 (b). Therefore, we propose that growing GaSb QDs on the (2x8) surface reconstruction in the manner described here increases the morphological stability of the QDs and may make them more resistant to dissolution upon capping.

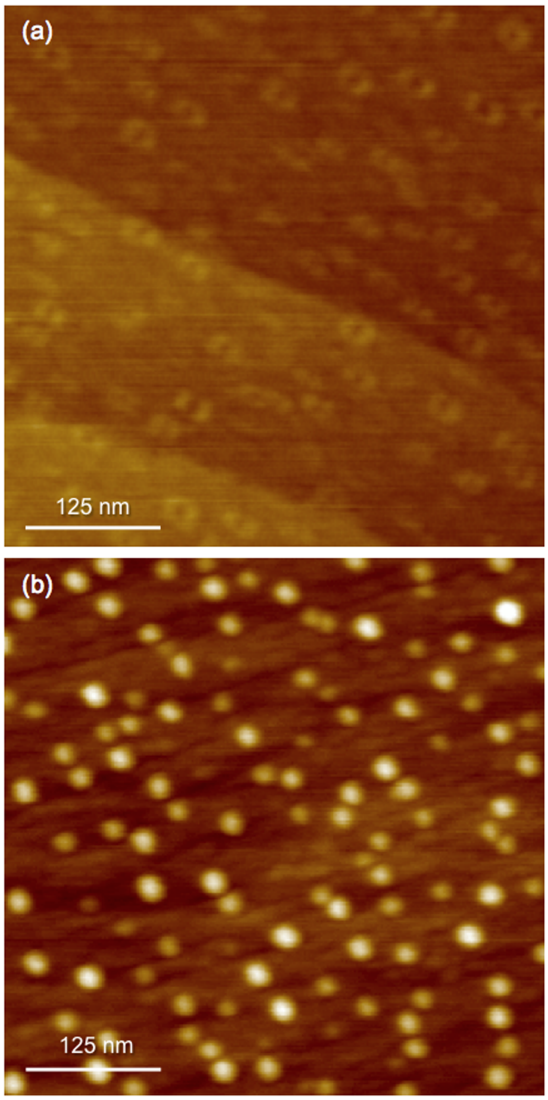

Figure 6.5: AFM images of QDs from the single layer samples grown on (a) the (2x4) surface and (b) the (2x8) surface showing the resulting QD morphology after quenching in the absence of a group V overpressure. The height scale is 6 nm.

6.4 Conclusions

GaSb QDs grown on the Sb-terminated (2x8) surface reconstruction were shown to be smaller, have a higher width/height aspect ratio, and a higher areal density than those grown on the As-terminated (2x4) surface. High resolution HAADF images show defect-free QD/spacer

layer interfaces for samples grown on both starting surfaces and non-compact dots, which may be due to dissolution and/or quantum ring formation upon capping. Additionally, the QD and WL photoluminescence peaks were at the same energies of 1.13 and 1.35 eV for dots grown on both surfaces despite the difference in QD size and shape. QDs grown on the (2x8) surface demonstrated higher morphological stability in the absence of Sb during post-growth quench.

6.5 References

[1] A. Luque, and A. Marti, *Phys. Rev. Lett*. **78** 26 5014 **(**1997).

[2] A. Marti, L. Cuadra, and A. Luque, Proc. Of the 28th IEEE Photovoltaics Specialists Conference, IEEE, New York (2000) p. 940.

[3] L. Cuadra, A. Marti, and A. Luque, *Physica E* **14**, 162-165 (2002).

[4] A. Marti, N. Lopez, E. Antolin, E. Canovas, C. Stanley, C. Farmer, L. Cuadra, and A. Luque, *Thin Solid Films* **511-512**, 638-644 (2006).

[5] M. Geller, C. Kapteyn, L. Muller-Kirsch, R. Heitz, and D. Bimberg, *Appl. Phys. Lett*. **82** 16 (2003).

[6] N.N. Ledentsov, V.A. Shchukin, M. Grundmann, N. Kirstaedter, J. Bohrer, O. Schmidt, D. Bimberg, V.M. Ustinov, A.Yu. Egorov, A.E. Zhukov, P.S. Kop'ev, S.V. Zaitsev, N.Yu. Gordeev, Zh.I. Alferov, A.I. Borovkov, A.O. Kosogov, S.S. Ruvimov, P. Werner, U. Gosele, and J. Heydenreich, *Phys. Rev. B* **54** 12 8743 (1996).

[7] L. Bousaiene, B. Ilahi, L. Sfaxi, F. Hassen, H. Maaref, O. Marty, and J. Dazord, *Appl. Phys. A* **79** 587-591 (2004).

[8] G. Balakrishnan, J. Tatebayashi, A. Khoshakhlagh, S. H. Huang, A. Jallipalli, L. R. Dawson, and D. L. Huffaker, *Appl. Phys. Lett*. **89**, 161104 (2006).

[9] S. Huang, G. Balakrishnan, and D. L. Huffaker, *J. Appl. Phys*. **105**, 103104 **(**2009).

[10] Xie, Q., Madhukar, A., Chen, P., and Kobayashi, N.P., *Phys. Rev. Lett*. **75** 2542-2545 (1995).

[11] Kiravittaya, S., Rastelli, A., Schmidt, O.G., *Rev. Prog. Phys.*, **72**, 046502 (2009).

[12] J. E. Bickel, C. Pearson, and J. M. Millunchick, *Surface Science* **603**, 14-21 (2009).

[13] J. E. Bickel, N. Modine, J. M. Millunchick, *Surface Science* **603**, 2945-2949 (2009).

[14] R. Timm, H. Eisele, A. Lenz, L. Ivanova, G. Balakrishnan, D. L. Huffaker, and M. Dahne, *Phys. Rev. Lett*. **101**, 256101 (2008).

[15] R. Timm, A. Lenz, H. Eisele, L. Ivanova, M. Dahne, G. Balakrishnan, D. L. Huffaker, I. Farrer, and D. A. Ritchie, J. *Vac. Sci. Technol. B* **26**(4) 1492 (2008).

[16] M. A. Kamarudin, M. Hayne, R. J. Young, Q. D. Zhuang, T. Ben, and S. I. Molina, *Phys. Rev. B* **83**, 115311 (2011).

[17] R. Timm, H. Eisele, A. Lenz, L. Ivanova, V. Vosseburger, T. Warming, D. Bimberg, I. Farrer, D. A. Ritchie, and M. Dahne, *Nano Lett.* **10**, 3972-3977 (2010).

[18] J. Tatebayashi, B. Liang, D. A. Bussian, H. Htoon, S. Huang, G. Balakrishnan, V. Klimov, L. R. Dawson, and D. L. Huffaker, *IEEE Transactions on Nanotechnology* **8**, 2 269 **(**2009).

[19] F. Hatami, N. N. Ledentsov, M. Grundmann, J. Bohrer, F. Heinrichsdorff, M. Beer, D. Bimberg, S. S. Ruvimov, P. Werner, U. Gosele, J. Heydenreich, U. Richter, S. V. Ivanov, B. Ya. Meltser, P. S. Kop'ev, and Zh. I. Alferov, *Appl. Phys. Lett*. **67**, (5) 656 (1995).

[20] B. R. Bennett, M. E. Thibado, M. E. Twigg, E. R. Glaser, R. Magno, B. V. Shanabrook, and L. J. Whitman, *J. Vac. Sci. and Tech. B* **14/3**, 2195-2198 (1996).

[21] E.R. Glaser, B.R. Bennett, B.V. Shanabrook, R. Magno, *Appl. Phys. Lett.* **68** (25) 3614 (1996).

Chapter 7

The Disintegration of GaSb/GaAs Nanostructures Upon Capping

Atom probe tomography and cross-sectional scanning tunneling microscopy show that GaSb/GaAs quantum dots disintegrate into ring-like clusters of islands upon capping. Band transition energies calculated using an 8-band **k.p** model of the capped dots with the observed dimensions are consistent with emission energies observed in photoluminescence data. These results emphasize the need for full three-dimensional characterization to develop an accurate understanding of the structure, and thus the optical properties, of buried quantum dots.

7.1 Introduction

Semiconductor quantum dots (QDs) are of particular interest for electronic applications such as photovoltaics,[1-4] lasers,[5,6] and charge storage devices.[7] Specifically, GaSb/GaAs QDs are of interest because of their type-II band alignment, which is believed to increase charge separation and reduce radiative recombination, making them a primary candidate for intermediate band solar cells.[3] For device applications, QDs are capped following their formation. The specific materials used for the dot and capping layer[8] as well as the particular capping conditions (*e.g.*, temperature, growth rate)[9,10] can affect the size, shape, and composition of buried QDs. For example, dissociation and a change in QD shape for GaSb/GaAs QDs has been observed due to intermixing between the capping material and the QD.[11-18] This redistribution of the QD material upon capping affects the optical properties of the dots by

creating large variations in the size and composition of the capped QDs, leading to an undesirable increased photoluminescence (PL) linewidth.[13,16,19-21]

Understanding the three-dimensional structure of buried QDs and the subsequent effects on their optoelectronic properties is fundamental to determining ways to either exploit or eliminate changes in shape and/or composition that occur to GaSb/GaAs QDs during capping. Several studies have investigated capped QD composition and morphology by using two-dimensional analytical techniques such as transmission electron microscopy (TEM)[14,16,17] and cross-sectional scanning tunneling microscopy (XSTM).[11-16] To date, capped GaSb/GaAs nanostructures have been hypothesized to evolve into rings.[11-17] XSTM, which images a single *x*-*z* plane of the nanostructure, shows that many, though not all of the QDs change into pairs of small islands separated by 5 to 10 nm of pure GaAs. The pairs of small islands have been interpreted as the body of the ring with a GaAs-filled center between them.[11-15] There are also some reports of this ring structure in TEM studies,[14,16,17] but because TEM relies on projections through the thickness of the nanostructures, it is difficult to distinguish the pairs of islands as seen in XSTM. More recently, XSTM has shown that small clusters of GaSb may form upon capping.[15] Given this ambiguity, the range of structures observed in capped GaSb still needs to be further understood.

These nanostructures can be studied using atom probe tomography (APT), which provides three-dimensional information about their shape and composition. Combining XSTM and APT provides a clearer understanding of the structure of the buried QDs and offers further explanation for the optical properties observed for these nanostructures. This chapter presents analysis of buried GaSb/GaAs QDs via XSTM and APT, and discuss the effects of

compositional and morphological changes incurred during capping on the optoelectronic properties of the nanostructures as seen in the QD PL and band transition energy calculations.

7.2 Experimental Procedure

A multilayer GaSb/GaAs sample with eleven QD layers was grown by molecular beam epitaxy on a GaAs(100) substrate for PL and atomic force microscopy (AFM) analysis. A 500 nm thick undoped GaAs buffer layer was grown at T = 590 ^{o}C at a rate of 1.0 monolayer (ML) s^{-1}. The sample was then cooled to T = 460 ^{o}C for deposition of 2.3 ML of GaSb at a rate of 0.3 MLs^{-1} and a V/III ratio of 2, immediately followed by a 20 nm GaAs spacer layer grown at the same rate. QDs were formed via the Stranski-Krastanov growth mode whereby a thin, uniform GaSb layer called the wetting layer (WL) is initially formed and QDs nucleate to decrease the overall strain once a critical thickness of GaSb is deposited. All temperatures were measured using an optical pyrometer. The topmost (eleventh) layer remained uncapped for analysis by AFM for comparison to the capped nanostructures. PL measurements were taken at T = 10 K in a helium flow cryostat at 424.5 μW using a HeNe laser operating at 633 nm. The PL spectrum was collected using a 0.75 m spectrometer with a 150 G/mm reflection grating and a single channel InGaAs detector.

A second sample was grown for XSTM and APT under the same conditions as the first (*i.e.*, same growth rates, temperatures, and amount of GaSb deposited for the QDs). However, the number of GaSb/GaAs QD layers was reduced to five and the spacer thickness increased to 50 nm to reduce strain build up in order to get a smoother cleaved surface for XSTM. Additionally, the buffer and topmost GaAs layer were p-doped to a concentration of 1 x 10^{17} cm^{-3}. XSTM measurements were performed at T = 77 K under ultra-high vacuum conditions ($p \leq 3$ x 10^{-11} mbar). Electrochemically etched tungsten tips were operated at constant current mode in the

STM. The samples were cleaved in-situ to scan over atomically flat and clean (110) surfaces. The APT volumes were prepared using a standard focused ion beam lift-out technique[22] and annularly milled to a tip diameter of approximately 100 nm at the apex. Analysis was done in a LEAP 4000X operated between 20 and 33 K in voltage pulsing mode with a pulse fraction of 15%. Six APT volumes, each consisting of one or two QD layers, were obtained. Reconstruction parameters (*i.e.*, image compression factor and the value of the evaporation field) were selected to yield flat GaSb layers and to match the layer spacing of 50 nm. Volumes where only a single GaSb layer was imaged were reconstructed using the same evaporation field, and only minor changes were made to the image compression factor to ensure a flat GaSb layer.

7.3 Data Analysis

7.3.1 QD Dimensions and Photoluminescence

Uncapped surface QDs were imaged by AFM to compare the size and areal density of the buried dots to their uncapped precursors. Figure 7.1 shows an AFM image of the uncapped QDs and histograms of the dot diameter and height size distributions. The number of bins for the histograms was determined based on the square root of the total number of data points. The average diameter and height of the uncapped QDs are 42 ± 5 nm and 3.6 ± 0.9 nm, respectively, and the areal density of QDs is 3.5 x 10^{10} cm^{-2}. Figure 7.2 shows the PL spectrum from the eleven-layer QD sample. The GaAs substrate peak is at 1.49 eV, the WL peak is at 1.36 eV, and the QD peak is centered at approximately 1.13 eV. The QD peak appears to have a shoulder at approximately 1.18 eV, and it has two lower energy peaks at 0.98 and 1.07 eV, all of which are unexpected because the size distribution of the uncapped QDs as measured by AFM appears to

follow a normal distribution (Figure 7.1 (b) and (c)). Instead, it is likely that the inhomogeneity in the PL results from changes in the QD shape and size upon capping.[20]

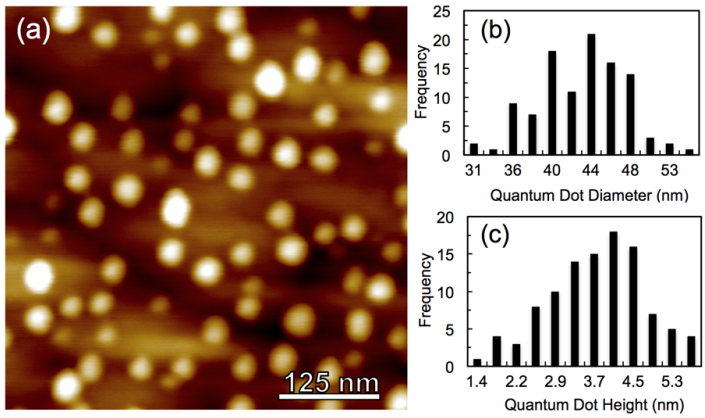

Figure 7.1: (a) AFM image of the uncapped GaSb/GaAs QDs. (b) and (c) Histograms of the QD diameter and height size distributions, respectively, for the uncapped QDs.

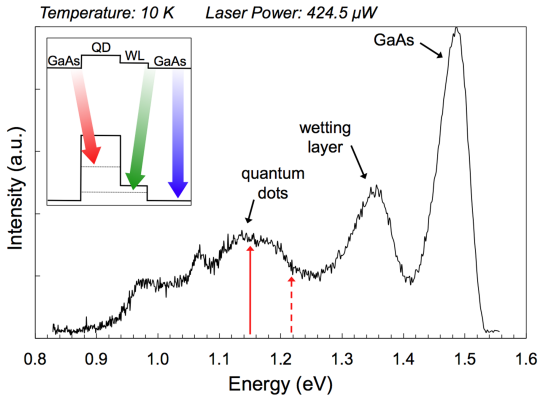

Figure 7.2: PL taken at 10 K and 424.5 μW of the GaSb/GaAs QDs showing the GaAs substrate peak at 1.49 eV, the WL peak at 1.36 eV, and the QD peak centered between 1.1 and 1.22 eV. The solid and dashed red arrows indicate the peak positions calculated for large compact QDs (1.155 eV) and small, disintegrated islands (1.220 eV) using an 8-band **k.p** method where approximate nanostructure dimensions are taken from the APT data. The inset shows the recombination pathways for the GaSb QDs, GaSb WL, and GaAs. Data collected by Timothy W. Saucer and Garrett V. Rodriguez, Prof. Vanessa Sih group, Physics Department, University of Michigan.

7.3.2 Two-dimensional Analysis of Buried Nanostructures

The buried QDs were analyzed by XSTM in order to gain information about their size, shape, and composition after capping. XSTM images of the various types of nanostructures observed are shown in Figure 7.3. Three primary structures can be identified via XSTM: compact QDs, pairs of small islands, and clusters of islands, in agreement with other reports.[15] The formation of island pairs and clusters was attributed to the relaxation of strain caused by the lattice mismatch of the GaSb and GaAs, and the clusters were assumed to be an intermediate structure.[15] Assuming that the island pairs and clusters form from dissociation of compact QDs and are, therefore, counted as single nanostructures, the areal density of nanostructures as measured by XSTM is approximately 2×10^{10} cm^{-2}, which is in good agreement with the density of the uncapped QDs as measured by AFM. Figure 7.3 (a) shows an XSTM image of a compact QD with a truncated pyramidal shape. Figure 7.3 (b) and (c) show island pairs with spacings between islands of approximately 2 and 15 nm, respectively. In addition to compact dots and rings, clusters similar to those reported by Smakman *et al.* are also observed.[15] Figure 7.3 (d) and (e) show examples of clusters, which we define as groups of small islands that appear to arise due to the dissolution of QDs upon capping. These clusters differ from the island pairs in their number of segments and/or the spacing between segments, which may be as small as a few atoms.

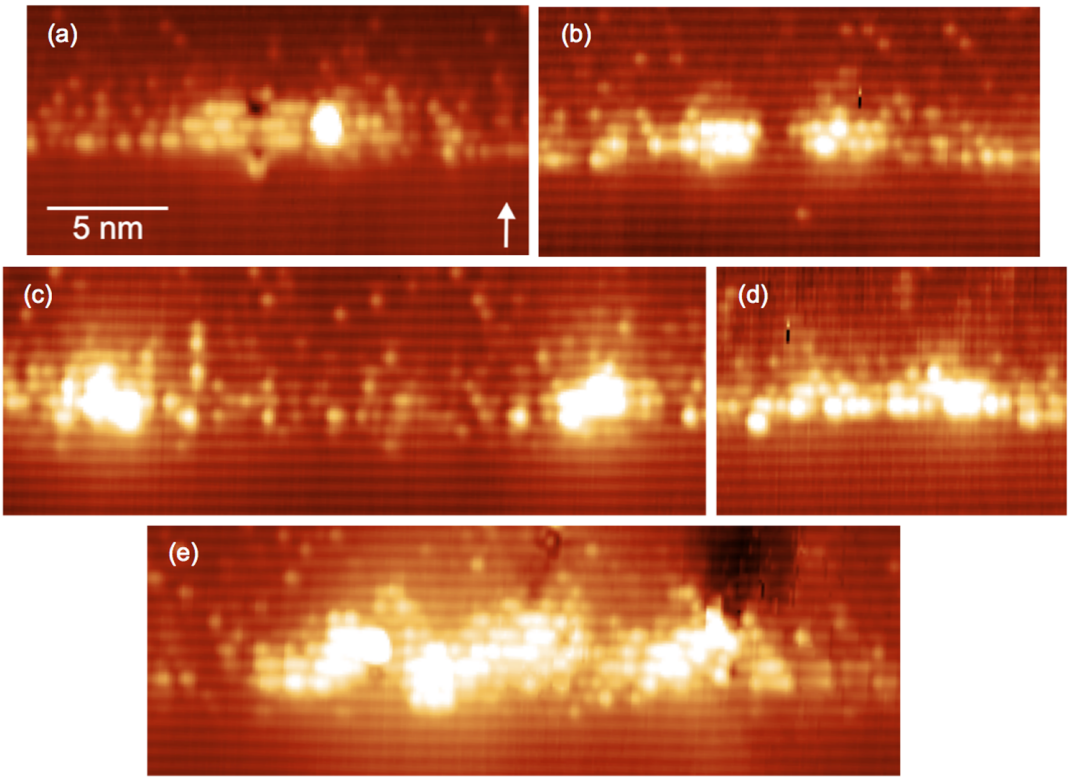

Figure 7.3: XSTM images of the GaSb/GaAs nanostructures looking at (110) surfaces showing (a) a compact QD, (b) – (e) clusters of smaller islands with varying separation and degrees of As-Sb intermixing between the islands. Images taken by Erwin Smakman, Prof. Paul Koenraad group, Eindhoven University of Technology, The Netherlands.

7.3.3 Three-dimensional Analysis by Atom Probe Tomography

APT analysis of the nanostructures in three-dimensions is used in conjunction with the XSTM data to gain further understanding of the morphology of the buried QDs. The nanostructures observed by APT are consistent with those observed in the XSTM images. Figure 7.4 shows a three-dimensional plot of one of the APT volumes showing two GaSb nanostructures. Figure 7.4 also shows several contour plots of Sb concentration for some of the capped GaSb nanostructures analyzed by APT. The three-dimensional plot in Figure 7.4 (a) shows only Sb atoms. An iso-concentration surface of approximately 9% Sb is highlighted. The

contour plots in Figure 7.4 (b) – (e) are created by slicing through the center of the nanostructures. The concentration scale is the same for each contour plot and is based on three-dimensional iso-concentration surfaces. A voxel size of 0.5 x 0.5 x 0.5 nm^3 and a delocalization distance of 3 nm are used. The choice of these parameters only affects the smoothness of the profiles and not the local concentrations that each region represents. The images in Figure 7.4 are intended to be qualitative. Lower Sb concentrations in Figure 7.4 are displayed in color from darker (lower %Sb) to lighter (higher %Sb). Higher Sb concentrations in the compact QD in Figure 7.4 (c) are simply shown in white with black contours. One-dimensional profiles are obtained along cylinders of 1.5 nm diameter with a bin width of 1.5 nm, and shown in Figure 7.5 to provide quantitative values of Sb concentration. The locations of the line profile locations through the nanostructures are indicated by (1), (2), and (3) in Figure 7.4. In contrast to what is suggested by the XSTM images, all examined APT volumes show that there are only two major types of buried nanostructures: compact QDs and ring-like clusters of small islands. Compact QDs account for approximately one third of the nanostructures observed while clusters of small islands account for the rest. Each cluster is comprised of two to four islands, which vary in size and shape. The concentration of Sb between the islands of each cluster also varies. For example, there is more Sb present between the islands in the cluster in Figure 7.4 (b) than there is between those shown in Figure 7.4 (c) and (d) (note that Figure 7.4 (d) shows two side-by-side clusters of small islands). Nonetheless, for all clusters of small islands, the concentration of Sb is consistently lowest at their center, providing a 'ring-like' shape. From the line profiles in Figure 7.5, we see that the concentration of the compact QDs reaches approximately 50% Sb at the center and decreases outward due to intermixing during capping. However, the small islands

within the clusters are much more dissociated, and the Sb concentration at the center in (3) is on the order of that of the WL.

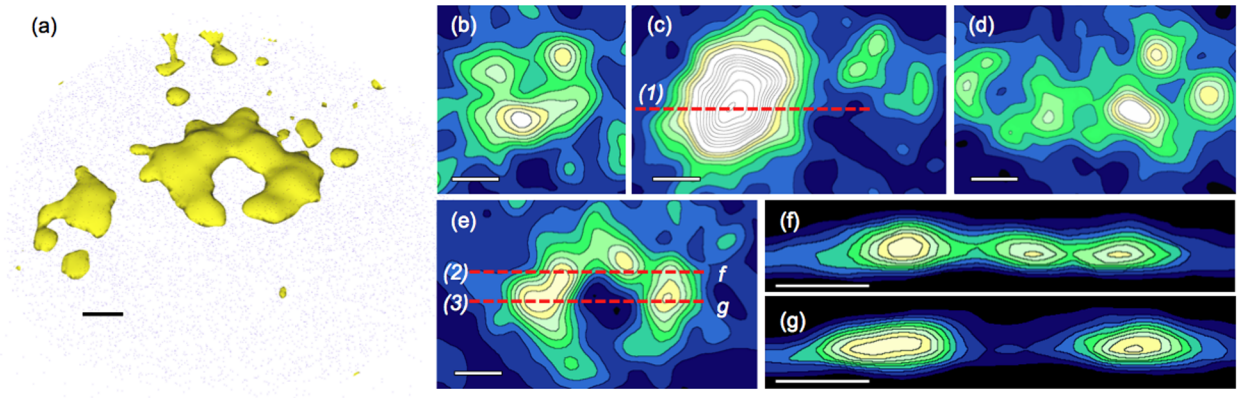

Figure 7.4: (a) Three-dimensional image of one of the APT volumes showing only Sb atoms. Yellow iso-concentration surfaces highlight areas with 9% Sb concentration. (b) – (e) Contour plots of varying Sb concentration composed from a slice through the center of the nanostructures as analyzed by APT. The concentration scale is the same for each plot. A voxel size of 0.5 x 0.5 x 0.5 nm^3 and a delocalization distance of 3 nm were used. Sb concentrations are displayed in color from darker (lower %Sb) to lighter (higher %Sb). Higher concentrations shown in the compact QD in (c) are displayed in white with black contour lines. Note that (d) contains two side-by-side clusters of small islands. (f) and (g) Cross-sectional views along a given *x-z* plane taken from (e). (1), (2), and (3) are described in Figure 5. All scale bars are 5 nm. APT data collected by Prof. Emmanuelle Marquis, MSE Department.

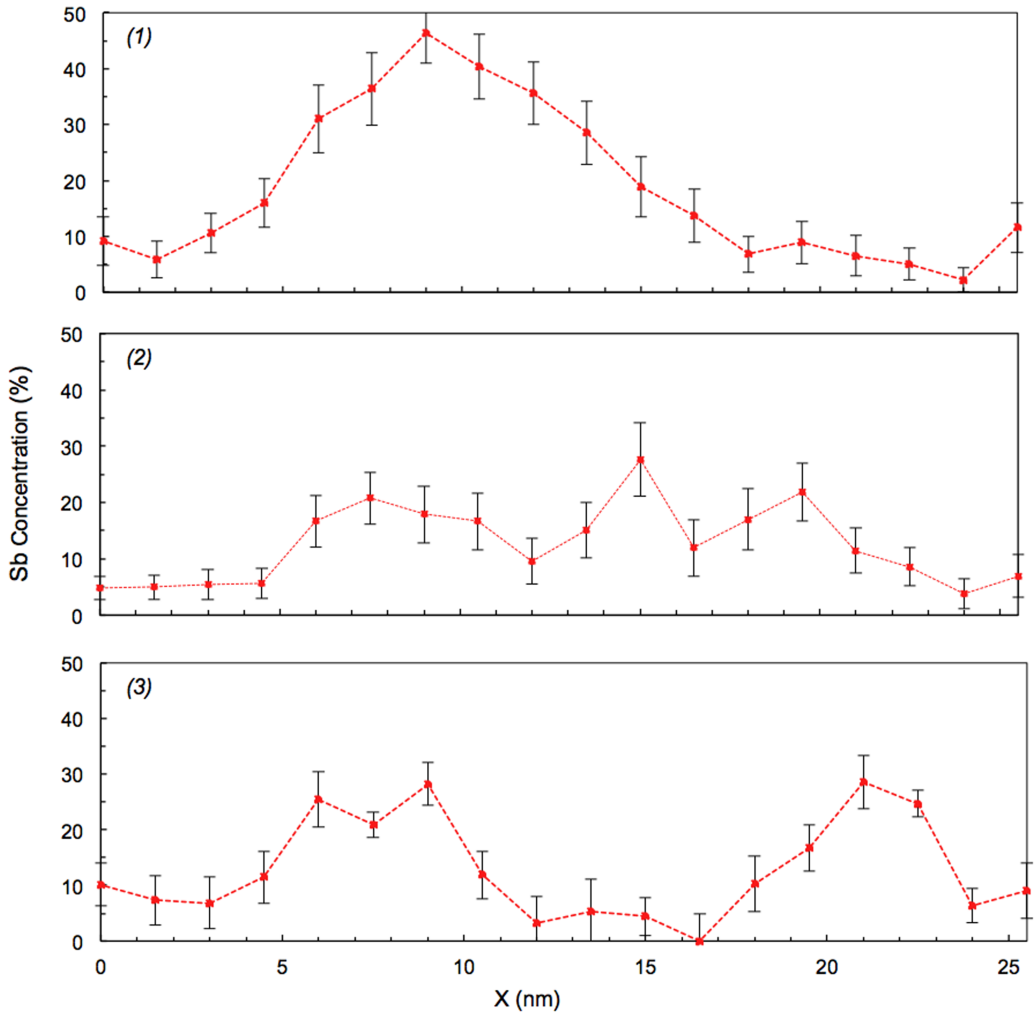

Figure 7.5: Line profiles of Sb concentration measured through the center of the nanostructures at locations (1), (2), and (3) in Figure 4(c) and (e) using a cylinder with a diameter of 1.5 nm and a 1.5 nm bin width. The dashed line in each plot is a guide to the eye.

Cross-sectional contour plots of Sb concentration shown in Figure 7.4 (f) and (g) are taken from slices along different *x*-*z* planes through the same ring-like cluster of small islands (Figure 7.4 (e)). These cross-sectional contours provide a view of the sample analogous to what is imaged using XSTM. By comparing Figure 7.4 (f) and (g), it becomes obvious that the position of the cross-section within the cluster of small islands greatly affects the interpretation

of the image when viewed solely along a specific *x-z* plane. For example, Figure 7.4 (f) shows a cluster very similar to the XSTM image in Figure 7.3 (e), while Figure 7.4 (g) shows a pair of small islands very similar to the XSTM image in Figure 7.3 (c) even though these two cross sections taken from Figure 7.4 (e) are only a handful of atomic spacings apart. It is clear, therefore, that GaSb QDs do not simply form rings upon capping as previously hypothesized. Rather, the QDs disintegrate into smaller islands. This fact can only be determined without ambiguity using a three-dimensional characterization technique such as APT. One drawback of this method, however, is the small number of nanostructures that can be analyzed at one time. Therefore, other nano-scale techniques like XSTM and TEM are necessary in order to analyze a larger number of nanostructures. This provides improved statistics on the size and type of nanostructures present. For instance, in this work each APT sample contained two to four complete nanostructures (*i.e.*, nanostructures completely encompassed within the APT volume as opposed to partially imaged nanostructures at the edge of the volume), while TEM and XSTM can provide an order of magnitude more structures per image. Combining these techniques provides a clearer interpretation of the three-dimensional morphology of the capped nanostructures than any one technique alone.

7.3.4 Calculated Transition Energies of Disintegrated QDs

The evolution of the QDs during capping significantly affects the optical properties of the buried nanostructures as evidenced by the PL (Figure 7.2). We propose that the broadening of the QD PL peak results from a distribution of compact QDs and clusters of small islands formed during capping. We estimate the effect of the compact QDs and clusters of smaller islands by comparing their transition energies, calculated using an 8-band **k.p** model.[23] In the calculation,

the shape of the compact QD and the smaller islands within the clusters are defined as spherical caps. The diameter and height of the compact QDs, estimated based on the APT data, are 21 nm and 3.6 nm, respectively. The diameter and height of the small islands are 13 nm and 2.3 nm, respectively. The strain distribution in GaSb/GaAs nanostructures was calculated using the valence force field model of Martin.[24] With the atomic displacement of minimal total energy condition, the deformation potential of the structure was calculated[25] to construct the strain Hamilton. In this step, the conduction band, heavy-hole, light-hole, and spin-orbit bands of GaSb are shifted down to 530 meV to obtain consistency with the experimental value of the transition energy within the QDs[26] and the conduction band offset of the QDs.[27] The total 8-band **k.p** Hamiltonian[23,28] was numerically solved by the finite difference method to obtain the hole states in the valence band. The transition energies calculated were 0.365 and 0.300 eV for the compact QDs and smaller islands, respectively, resulting in PL peaks at 1.155 and 1.220 eV, as indicated by the solid and dashed lines in Figure 7.2. These energies are in reasonable agreement with the broadening of the PL peak and support the hypothesis that QD disintegration upon capping leads to a broadening, and in this case, a bimodal distribution of QD sizes due to the presence of compact QDs and small islands. The origin of the two lowest energy peaks remains uncertain. Based on these calculations, it is unlikely that the two lowest energy peaks also result from inhomogeneity in QD size because the dot dimensions required for emission at such low energies are larger than that of their uncapped precursors, let alone accounting for any size reduction resulting from intermixing during capping. We observe that these two peaks have a narrow line width and are approximately equidistant from the two peaks between 1.1 and 1.2 eV, suggesting that they may arise due to impurity states within the QDs, although their origin is yet unknown.

7.4 Conclusions

In conclusion, we have demonstrated by three-dimensional analysis via APT that GaSb/GaAs QDs disintegrate into ring-like clusters of small islands upon GaAs capping with approximately two to four islands per cluster. These ring-like clusters appear as closely spaced island pairs or clusters when imaged by XSTM, demonstrating the need for multiple corroborative techniques in order to fully understand the structure of buried QDs. The presence of clusters and compact dots results in a broad size distribution of nanostructures, and in this particular case, a bimodal size distribution. This is evident in the split QD PL peak and corroborated by the calculated transition energies for the compact QDs and small islands within the clusters using an 8-band **k.p** model.

7.5 Applications of GaSb Quantum Dots

The fabrication and study of p-n and p-i-n junction solar cells containing III-V semiconductor QDs is a growing area of research. Initial studies in this area implemented InAs/GaAs QDs because their growth was well studied.[4] Later studies turned to GaSb/GaAs QDs because of their type-II band alignment, which was theorized to decrease radiative recombination and increase charge separation.[29-31] The understanding of the effects of growth conditions and capping of GaSb QDs gained from these studies was used to fabricate p-i-n and p-n junction solar cells containing GaSb QDs for increased infrared spectral response. This work was done in collaboration with Prof. Jamie Phillips and his group in the Department of Electrical Engineering.

QDs grown on the Sb-terminated (2x8) surface were found to have a higher areal density and brighter PL emission, making them more advantageous than dots grown on the As-

terminated surface reconstruction. Admittance spectroscopy[32] done by collaborators confirmed good carrier confinement in the GaSb QDs and measured their activation energy and capture cross-section. Admittance spectroscopy also showed that the thermal emission rates of GaSb/GaAs QDs were much lower than their type-I counterparts. Therefore, GaSb QDs grown on the (2x8) surface were used for all QD solar cells. The growth details of the QDs, their position with respect to the junction, and the details of the device structure were all varied in order to find the best structure for increasing the short circuit current while retaining a high open circuit voltage. Increasing the GaSb thickness above 3.0 ML was found to increase the areal density of the dots, theoretically providing increased absorption in the infrared regime. However, the subsequent increase in dot size was found to result in defect formation in the layers immediately above the dots, which carried into the emitter region and hindered device efficiency. Therefore, the GaSb thickness was reduced to 2.3 ML, nearly eliminating defects completely. Solar cells with a p^+n structure containing five layers of GaSb QDs were fabricated, achieving an efficiency of 12.61%. Figure 7.6 and Figure 7.7 shows the current-voltage and external quantum efficiency, respectively, for structures with the QDs placed in different locations with respect to the junction.[33] Increased absorption in the infrared regime was observed due to the GaSb QDs for a device structure with the dots placed within the junction (Figure 7.7). Although the efficiency of the QD solar cell was below that of the control cell (18.26%), it achieved the highest efficiency to date for a GaSb QD solar cell. Further studies related to QD growth and capping may improve upon solar cell efficiency.

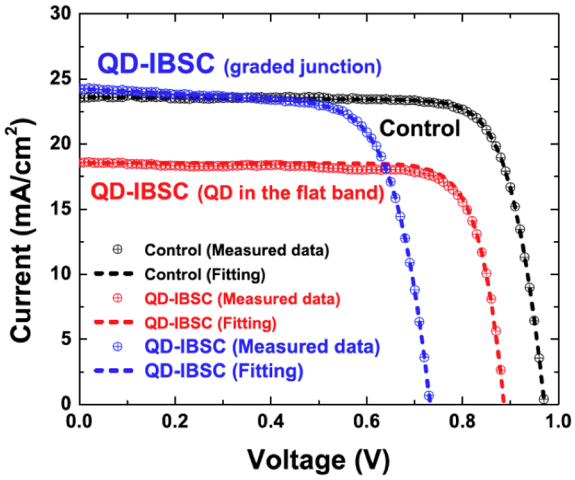

Figure 7.6: Current-voltage plots for QD intermediate band solar cells with QDs outside the junction and inside the junction. Figure taken from abstract accepted to the IEEE Photovoltaic Conference 2013.[33] Data measured by Jinyoung Hwang, Prof. Jamie Phillips group, Electrical Engineering Department, University of Michigan.

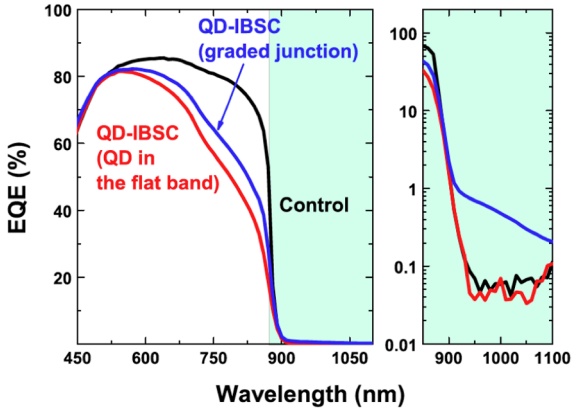

Figure 7.7: External quantum efficiency (EQE) plot showing the enhanced absorption resulting from QDs placed inside the junction. Figure taken from abstract accepted to the IEEE Photovoltaic Conference 2013.[33] Data measured by Jinyoung Hwang, Prof. Jamie Phillips group, Electrical Engineering Department, University of Michigan.

7.6 References

[1] A. Luque and A. Marti, *Phys. Rev. Lett.* **78** 26 5014 **(**1997).

[2] A. Marti, L. Cuadra, and A. Luque, Proc. Of the 28th IEEE Photovoltaics Specialists Conference, *IEEE*, New York, 2000, p. 940.

[3] L. Cuadra, A. Marti, and A. Luque *Physica E* **14** 162 (2002).

[4] A. Marti, N. Lopez, E. Antolin, E. Canovas, C. Stanley, C. Farmer, L. Cuadra, and A. Luque, *Thin Solid Films* **511-512**, 638 (2006).

[5] N. N. Ledentsov, V. A. Shchukin, M. Grundmann, N. Kirstaedter, J. Bohrer, O. Schmidt, D. Bimberg, V. M. Ustinov, A. Yu. Egorov, A. E. Zhukov, P. S. Kop'ev, S. V. Zaitsev, N. Yu. Gordeev, Zh. I. Alferov, A. I. Borovkov, A. O. Kosogov, S. S. Ruvimov, P. Werner, U. Gosele, and J. Heydenreich, *Phys. Rev. B* **54** 12 8743 (1996).

[6] L. Bousaiene, B. Ilahi, L. Sfaxi, F. Hassen, H. Maaref, O. Marty, and J. Dazord, *Appl. Phys. A* **79** 587 (2004).

[7] M. Geller, C. Kapteyn, L. Muller-Kirsch, R. Heitz, and D. Bimberg, *Appl. Phys. Lett.* **82** 16 (2003).

[8] J. M. Ulloa, R. Gargallo-Caballero, M. Bozkurt, M. del Moral, A. Guzman, P. M. Koenraad, and A. Hierro, *Phys. Rev. B* **81** 165305 (2010).

[9] Q. Gong, P. Offermans, R. Notzel, P. M. Koenraad, and J. H. Wolter, *Appl. Phys. Lett*. **85** 23, 5697 (2004).

[10] J. M. Ulloa, C. Celebi, P. M. Koenraad, A. Simon, E. Gapihan, A. Letoublon, N. Bertru, I. Drouzas, D. J. Mowbray, M. J. Steer, and M. Hopkinson, *J. of Appl. Phys.* **101** 081707 (2007).

[11] R. Timm, H. Eisele, A. Lenz, L. Ivanova, G. Balakrishnan, D. L. Huffaker, and M. Dahne, *Phys. Rev. Lett*. **101** 256101 (2008).

[12] R. Timm, A. Lenz, H. Eisele, L. Ivanova, G. Balakrishnan, D.L. Huffaker, I. Farrer, D. A. Ritchie, and M. Dahne, *J. of Vac. Sci. & Tech*. *B* **26(4)** 1492 (2008).

[13] R. Timm, H. Eisele, A. Lenz, L. Ivanova, V. Vosseburger, T. Warming, D. Bimberg, I. Farrer, D. A. Ritchie, and M. Dahne, *Nano Lett.* **10** 3972 (2010).

[14] M.A. Kamarudin, M. Hayne, R. J. Yound, Q. D. Zhuang, T. Ben, and S. I. Molina, *Phys. Rev. B* **83** 115311 (2011).

[15] E. P. Smakman, J. K. Garleff, R. J. Young, M. Hayne, P. Rambabu, and P. M. Koenraad, *Appl. Phys. Lett*. **100** 142116 (2012).

[16] R. J. Young, E. P. Smakman, A. M. Sanchez, P. Hodgson, P. M. Koenraad, and M. Hayne, *Appl. Phys. Lett*. **100** 082104 (2012).

[17] J. Tatebayashi, B. L. Liang, R. B. Laghumavarapu, D. A. Bussian, H. Htoon, V. Klimov, G. Balakrishnan, L. R. Dawson, and D. L. Huffaker, *Nanotechnology* **19** 295704 (2008).

[18] A. M. Beltran, E. A. Marquis, A. G. Taboada, J. M. Ripalda, J. M. Garcia, and S. I. Molina, *Ultramicroscopy* **111** 1073 (2011).

[19] G. Balakrishnan, J. Tatebayashi, A. Khoshakhlagh, S. H. Huang, A. Jallipalli, L. R. Dawson, and D. L. Huffaker, *Appl. Phys. Lett*. **89** 161104 (2006).

[20] A. J. Martin, T. W. Saucer, K. Sun, S. J. Kim, G. Ran, G. V. Rodriguez, X. Pan, V. Sih, and J. Millunchick, *J. of Vac. Sci. & Technol. B* **30(2)** 02B112 (2012).

[21] F. Hatami, M. Grundmann, N. N. Ledentsov, F. Heinrichsdorff, R. Heitz, J. Bohrer, D Bimberg, S. S. Ruvimov, P. Werner, V. M. Ustinov, P. S. Kop'ev, Zh. I. Alferov, *Phys. Rev. B* **57** 8 4635-4641 (1998).

[22] K. Thompson, D. Lawrence, D. J. Larson, J. D. Olson, T. F. Kelly, and B. Gorman, *Ultramicroscopy* **107** 131 (2007).

[23] H. Jiang and J. Singh *Phys. Rev. B* **56** 4696 (1997).

[24] R. M. Martin *Phys. Rev. B* **1** 4005 (1970).

[25] C. G. Van de Walle *Phys. Rev. B* **39** 1871 (1989).

[26] S. M. North, P. R. Briddon, M. A. Cusack, and M. Jaros *Physical Review B* **58** 12601 (1998).

[27] M. E. Rubin, H. R. Blank, M. A. Chin, H. Kroemer, and V. Narayanamurti *Appl. Phys. Lett* **70** 1590 (1997).

[28] K. Boujdaria, S. Ridene, and G. Fishman *Phys. Rev. B* **63** 235302 (2001).

[29] R. B. Laghumavarapu, A. Moscho, A. Khoshakhlagh, M. El-Emawy, L. F. Lester, and D. L. Huffaker *Appl. Phys. Lett.* **90** 173125 (2007).

[30] P. J. Carrington, A. S. Mahajumi, M. C. Wagener, J. R. Botha, Q. Zhuang, and A. Krier *Physica B: Condensed Matter* **407** 1493-1496 (2012).

[31] P. J. Carrington, M. C. Wagener, J. R. Botha, A. M. Sanchez, and A. Krier *Appl. Phys. Lett.* **101** 231101 (2012).

[32] J. Hwang, A. J. Martin, J. Millunchick, and J. D. Phillips *J. of Appl. Phys.* **101** 074514 (2012).

[33] J. Hwang, A. J. Martin, K. Lee, S. Forrest, J. Millunchick, and J. D. Phillips, Abstract accepted at *IEEE Photovoltaic Conference 2012.*

Chapter 8

Conclusions and Future Work

8.1 Summary and Conclusions

This work presents analysis of InAs and GaSb QDs with the intention of gaining a better understanding of QD properties under different conditions in order to take advantage of these properties in photonic crystals and QD solar cells. The first two studies demonstrate the ability to control QD position and size via *in vacuo* FIB patterning with up to 100% single QD per patterned site fidelity after six layers. The QD dimensions are directly controlled by the FIB-milled hole dimensions and pattern spacing. Additionally, the wetting layer thickness is also shown to change with changing pattern spacing. Analysis of the changes in dot dimensions with respect to pattern spacing provides a means of estimating the In adatom surface diffusion length during QD nucleation. Analysis of the PL with varying pattern spacing showed that the In diffusion length during dot nucleation is different form that of In during dot dissolution because the In atoms diffuse on different surfaces in these two cases (InAs surface during dot nucleation and a GaAs surface during dot dissolution). Increasing the total number of QD layers from six to 26 is detrimental to pattern fidelity due to mound formation above the patterned sites, and created a bimodal QD size distribution in this case for most larger pattern spacings as measured by AFM and evidenced by a split QD PL peak. The understanding about the relationship

between patterning conditions and dot properties is now being used in a collaborative effort to effectively place FIB-patterned InAs QDs within the optical cavity of a photonic crystal.

The other studies in this work focus on understanding how growth conditions affect GaSb QD properties in order to effectively implement them in QD solar cells. Sb segregation in GaSb quantum wells and dots is found to occur via two modes: strain-induced intermixing and surface segregation. The length scale of surface segregation is on the order of 2 nm and is much larger than that of strain-induced intermixing. Surface segregation dominates for the wetting layer surrounding the QDs due to excess Sb coming from disintegrating QDs during GaAs capping. The surface reconstruction of the QD nucleation surface is found to directly impact the size, areal density, and stability of the dots. GaSb QDs grown on the Sb-terminated (2x8) surface reconstruction are shown to be smaller, have a higher width/height aspect ratio, and a higher areal density than those grown on the As-terminated (2x4) surface. Photoluminescence spectra for samples growth on both starting surfaces are identical, although the QD signal is brighter or dots grown on the (2x8). Uncapped QDs grown on the (2x8) surface also demonstrate higher morphological stability in the absence of Sb during post-growth quench. Three-dimensional analysis of GaSb QDs grown on the (2x4) surface done by APT shows dot disintegration into ring-like clusters of small islands upon GaAs capping. This analysis provides a more complete understanding of how GaSb dot morphology changes during capping. The presence of clusters of smaller islands as well as some compact dots results in a broad size distribution of nanostructures, which is evident in the PL data and corroborated by the calculated transition energies for the compact QDs and small islands within the clusters using an 8-band **k.p** model. GaSb QDs were also effectively grown within a p-n junction solar cell in a collaborative effort, which achieved the highest efficiency GaSb QD solar cell to date.

8.2 Future Work

The next steps in this work primarily focus on the growth of GaSb QDs and their incorporation into intermediate band solar cells. While a fundamental understanding of GaSb dot disintegration has been reported, methods to either eliminate or exploit this phenomenon must be determined. There are several ways to theoretically affect the level of dissolution occurring during capping. It is important to note that the dissolution process must be time and energy dependent. Therefore, altering the capping rate, temperature, and/or capping material should impact the degree of QD disintegration.

It is difficult to alter the capping rate for GaSb QDs because the growth rate is limited by the group III material, which is Ga in the case of GaSb QDs. Since the GaAs cap is also rate-limited by Ga, the QDs and cap must be grown at the same rate. Since GaSb QDs are typically grown at a fairly slow rate (~0.3 MLs^{-1}), they are also capped at a fairly slow rate. If the dots are stable, then a growth interruption can be used to increase the temperature, and therefore the rate, of the Ga. As reported in this work, GaSb QDs are most stable when grown on the Sb-terminated (2x8) surface reconstruction.[1] A growth interruption may also introduce changes to dot size, shape, and/or areal density. Likewise, altering the capping temperature would also require a growth interruption while the sample temperature is adjusted. Despite the need for a short interruption for adjustment of the Ga cell or substrate temperature, capping at a faster rate and/or lower temperature remains a viable option for improving QD quality and retaining the uncapped shape and composition.

Using a different capping material has been shown to impede dissolution of InAs QDs.[2] More specifically, including small amounts of In or Sb in the GaAs capping layer has proven to preserve InAs dot size and shape. Preservation of the pyramidal QD shape was also shown to

affect the optoelectronic properties of the dots,[3] which is important for the intended applications of the studies presented in this work. Currently, new studies are beginning with the intention of analyzing the affects of capping QDs with a thin layer of AlAs as well as AlGaAs and GaAsSb. Samples will be analyzed using photoluminescence and cross-sectional scanning tunneling microscopy and compared to dots capped with GaAs. Ultimately, the goal is to implement promising structures into QD solar cells with the intention of improving efficiency as compared to recently fabricated solar cells.

In addition to improving current GaSb/GaAs QD solar cells, a collaborative effort is underway to use InAs QDs to make a hot carrier cell. InAs QDs grown on AlAsSb that is lattice matched to an InP substrate produce a type-II band alignment that has very recently come of interest[4] and may be advantageous for implementation in a hot carrier structure. In contrast to the GaSb/GaAs type-II band alignment, the major offset of the InAs/AlAsSb/InP structure is in the conduction band, while the valence band is relatively flat, make this material system more advantageous for a hot carrier design. This effort is in collaboration with Prof. Jamie Phillips group in Electrical Engineering. Initial AlAsSb films were grown with two layers of InAs QDs separated by 50 nm of AlAsSb. The most promising QD structure was grown using the following procedure. After desorbing the InP substrate, the optical pyrometer was calibrated for an InP substrate by finding the change in surface reconstruction that occured at approximately T = 470 ^{o}C and adjusting the emissivity of the pyrometer to set this transition to its known transition temperature of approximately T = 530 ^{o}C. A 400 nm AlAsSb film was then grown at T = 500 ^{o}C with an Al rate of 0.3 MLs^{-1} and As_2 and Sb rates of 1.0 MLs^{-1} each for approximately a 50%-50% As-Sb ratio in order to achieve a lattice matched film. The same temperature was used throughout the entire sample growth. A 50%-50% ratio was chosen because As has a tendency to

replace Sb during growth, therefore, a higher Sb flux is required to achieve the desired composition (likely closer to 60%-40%) necessary to lattice match the film to the InP substrate. Following AlAsSb film growth, 5.0 ML GaAs was deposited at 0.3 MLs^{-1}. 3.0 ML of InAs was deposited at a rate of 0.1 MLs^{-1} for the QDs. Following QD growth, 5 ML of GaAs was again deposited at a rate of 0.3 MLs^{-1} followed by a 50 nm AlAsSb spacer layer. A second layer of InAs QDs was grown with a 5 ML GaAs layer beneath it. The top layer of QDs remained uncapped for AFM analysis.

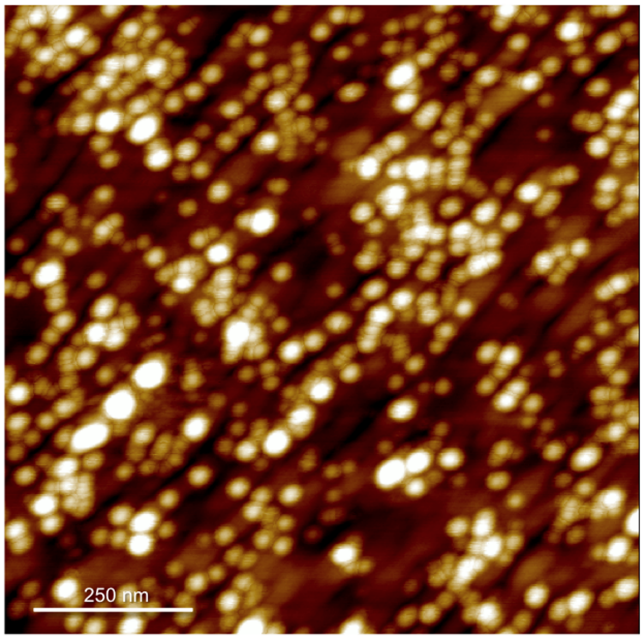

Figure 8.1: Atomic force microscope image of InAs QDs grown on lattice matched AlAsSb/InP.

Figure 8.1 shows an AFM image of the uncapped InAs dots. The QD size and areal density appear comparable to that of the GaSb QDs. However, 'streaks' in the underlying AlAsSb film are visible in the AFM images of the uncapped QDs. These 'streaks' may be the result of segregation in the film. Therefore, the quality of the AlAsSb film and the concentration of Sb required to lattice match the film to the InP substrate must be established prior to taking

further steps toward making devices. Figure 8.2 shows the PL spectrum from the film. The substrate peak is seen at 1.4 eV and a QD peak is seen at 1.15 eV. There is a shoulder on the substrate peak, which may arise due to the AlAsSb film on the InP, however, Omega-2 Theta scans of the film along (004) and (224) shown in Figure 8.3 do not show any shoulders. Further work to develop the AlAsSb/InP film growth is recommended prior to growing more QD samples or devices.

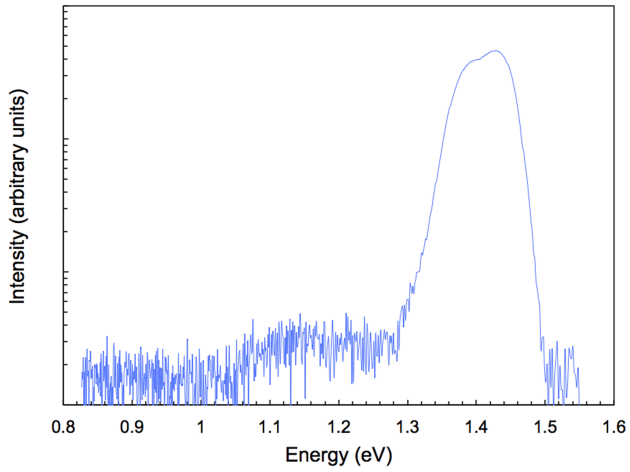

Figure 8.2: Photoluminescence spectrum for the InAs QDs on AlAsSb lattice matched to InP. The QD peak is seen at 1.15 eV and the substrate peak is at 1.4 eV. The shoulder on the substrate peak may be the result of the AlAsSb film.

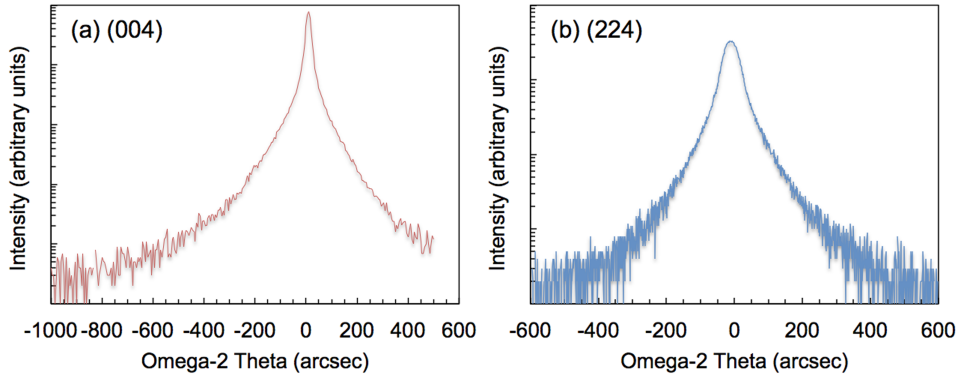

Figure 8.3: Omega-2 Theta scans of the InAs QDs on AlAsSb/InP for the (a) (004) and (b) (224) showing a single peak for each. Data collection assisted by Evan Anderson, Prof. Joanna Millunchick group, MSE Department.

8.3 References

[1] A. J. Martin, T. W. Saucer, K. Sun, S. J. Kim, G. Ran, G. V. Rodriguez, X. Pan, V. Sih, and J. Millunchick, *J. of Vac. Sci. & Technol. B* **30(2)** 02B112 (2012).

[2] J. M. Ulloa, C. Celebi, P. M. Koenraad, A. Simon, A. Letoublon, N. Bertru, I. Drouzas, D. J. Mowbray, M. J. Steer, and M. Hopkinson, *J. of Appl. Phys.* **101** 081707 (2007).

[3] J. M. Ulloa, I. W. D. Drouzas, P. M. Koenraad, D. J. Mowbray, M. J. Steer, H. Y. Liu, and M. Hopkinson, *Appl. Phys. Lett.* **90** 213105 (2007).

[4] P. J. Simmonds, R. B. Laghumavarapu, M. Sun, A. Lin, C. J. Reyner, B. Liang, and D. L. Huffaker, *Appl. Phys. Lett.* **100** 243108 (2012).